International Journal of Biological Macromolecules 229 (2023) 105–122

Contents lists available at ScienceDirect

International Journal of Biological Macromolecules

journal homepage: www.elsevier.com/locate/ijbiomac

Highly stretchable, adhesive, and biocompatible hydrogel platforms of tannic acid functionalized spherical nanocellulose for strain sensors

Dinesh K. Patel [a], Keya Ganguly [a], Sayan Deb Dutta [a], Tejal V. Patil [b], Aayushi Randhawa [b], Ki-Taek Lim [a,b,*]

[a] Department of Biosystems Engineering, Institute of Forest Science, Kangwon National University, Chuncheon 24341, Republic of Korea
[b] Interdisciplinary Program in Smart Agriculture, Kangwon National University, Chuncheon 24341, Republic of Korea

ARTICLE INFO

Keywords:
Adhesive
Self-healing
Shape memory
Biocompatibility
Strain sensor

ABSTRACT

The development of multifunctional wearable electronic devices has received considerable attention because of their attractive applications. However, integrating multifunctional abilities into one component remains a challenge. To address this, we have developed a tannic acid-functionalized spherical nanocellulose/polyvinyl alcohol composite hydrogel using borax as a crosslinking agent for strain-sensing applications. The hydrogel demonstrates improved mechanical and recovery strengths and maintains its mechanical strength under freezing conditions. The hydrogels show ultra-stretching, adhesive, self-healing, and conductive properties, making them ideal candidates for developing strain-based wearable devices. The hydrogel exhibits good sensitivity with a 4.75 gauge factor. The cytotoxicity of the developed hydrogels was monitored with human dermal fibroblast cells by WST-8 assay *in vitro*. The antibacterial potential of the hydrogels was evaluated using *Escherichia coli*. The hydrogels demonstrate enhanced antibacterial ability than the control. Therefore, the developed multifunctional hydrogels with desirable properties are promising platforms for strain sensor devices.

1. Introduction

The demand for smart wearable devices to develop electronic skins, soft robotics, and flexible sensors to monitor human motion and healthcare is increasing globally. Different properties, including flexibility, stretchability, deformability, and conductivity, are required to develop smart wearable electronic devices [1,2]. Zeng and coworkers fabricated transparent multifunctional polyacrylamide/starch-based hydrogels for humidity-sensing applications [3].

Adhesive hydrogels are suitable platforms for developing strain sensors that directly attach to the skin without using extra bandages or tapes. Jin et al. developed biocompatible, skin-attachable hydrogels for human motion and physiological signal monitoring [4]. The dopamine-based hydrogels exhibited enhanced adhesiveness with different surfaces due to the presence of highly reactive catechol groups. However, inorganic salts or conductive polymers are required in these hydrogels to achieve suitable electrical conductivity for sensing applications. It has also been observed that hydrogels combined with adhesiveness and conductivity exhibited poor toughness. Thus, it is still challenging to develop hydrogels integrated with the required adhesiveness, conductivity, and mechanical strength [5–7]. Significant efforts have been made to develop wearable electronic devices using silicon and metals. However, their broad applicability is restricted under mechanical deformation conditions owing to their adverse mechanical strength [8]. Any minor deformation, including cracks and scratches, adversely affects the normal function of the wearable sensor. Material with self-healing ability has additional advantages to making wearable electronic devices, which re-gains their original structure after the damage [9–11]. However, most developed materials require external stimuli for healing, including light, heat, and pressure. The dynamic supramolecular provides an alternative approach to form self-healing hydrogels at room temperature without using stimuli. Chen et al. developed an elastomer *via* a supramolecular approach with improved mechanical strength and self-healing potential under ambient conditions [12]. Yan et al. synthesized self-healing materials with enhanced stretchability through condensation polymerization [13].

Most synthesized materials lose their required properties, including mechanical strength, healing ability, stretching potential, and conductive properties, under adverse conditions, at low temperatures and acidic or basic conditions [14]. Therefore, synthesizing multifunctional

* Corresponding author at: Department of Biosystems Engineering, Institute of Forest Science, Kangwon National University, Chuncheon 24341, Republic of Korea.
E-mail address: ktlim@kangwon.ac.kr (K.-T. Lim).

https://doi.org/10.1016/j.ijbiomac.2022.12.286
Received 31 August 2022; Received in revised form 16 December 2022; Accepted 25 December 2022
Available online 29 December 2022

materials that can maintain their properties under adverse conditions is desirable for developing wearable electronic devices. Hydrogel ionotronics are considered suitable materials to make stretchable electronic devices owing to their attractive physicochemical properties. These hydrogels are composed of polymers and ionic conductors and are stabilized by weak interactions [15]. Borax-crosslinked polyvinyl alcohol (PVA) is an ideal hydrogel ionotronics owing to its biocompatibility and water solubility [16]. However, fabricating water-insoluble and water-encapsulated PVA/borax hydrogels remains challenging. Tannic acid (TA) is a naturally derived aromatic compound that contains an abundance of functional groups, such as hydroxyl (–OH) and carbonyl (–C═O), which facilitates the interaction with polymers through hydrogen and ionic bonding and hydrophobic and π–π interactions [17,18]. Furthermore, TA coordinates with different metal ions to generate metal-coordinated TA networks. However, the aggregation of TA in polymer solutions leads to catastrophic failure. This drawback can be overcome *via* the surface modification of TA.

Nanocellulose has received significant attention to use as a reinforcing agent because of its appealing physicochemical properties [19]. Based on their origin and structure, nanocellulose is categorized into cellulose nanofibrils (CNFs), cellulose nanocrystals (CNCs)/spherical nanocellulose (s-NC), and bacterial nanocellulose (BNC) [20]. The nanocellulose properties can be easily modified through surface functionalization. It is anticipated that s-NC has a higher surface area than its nanocrystal counterpart, which provides more reactive sites for functionalization. Considering the appealing potential of PVA and nanocellulose, the fabrication of nanocellulose-assisted PVA hydrogels may be diversely applied, including flexible sensors. The sensing abilities of nanocellulose-assisted and borax-crosslinked PVA hydrogels have been previously reported [21–25]. The enhancement in the physicochemical properties of the pure polymer has been previously reported with TA-modified CNCs [26,27]. However, the sensing potential of TA functionalized with shape-regulated nanocellulose has yet to be widely explored. We have previously reported accelerated wound healing using s-NC-mediated polymer patches [28].

This study explores the sensing abilities of TA-functionalized s-NCs and their effects on the physicochemical properties of PVA polymer. To the best of our knowledge, this is the first study to show the sensing ability of TA functionalized with shape-regulated nanocellulose/PVA hydrogel. The mechanical and rheological properties of the hydrogels were evaluated. The self-healing ability, stretchability, and recovery strengths of the developed hydrogels are also assessed. The developed hydrogels exhibit adhesive and conductive properties. The biocompatibility and antibacterial potential of the hydrogels are examined using human dermal fibroblast (HDF) cells and *Escherichia coli*, respectively. The strain-sensing abilities of the hydrogels are assessed at different human body parts, including finger, wrist, and leg bending. The strain sensitivity of the hydrogels is examined in terms of the gauge factors. Based on the results, we hypothesize that the developed multifunctional hydrogels have the potential for strain-sensing applications.

2. Materials and methods

2.1. Materials

The following chemicals were used as received without further purification: poly (vinyl alcohol) (PVA) (1500 DP, >99 %, Daejung Chemicals, Gyeonggi-do, Republic of Korea), potassium hydroxide, tannic acid, 4 % paraformaldehyde (PFA), bovine serum albumin (BSA), 4,6-diamino-2-phenylindole dihydrochloride (DAPI) (Sigma-Aldrich, St. Louis, MO, USA), sodium hydroxide (Junsei Chemicals, Tokyo, Japan), sodium chlorite, ammonium persulfate (APS) (Daejung Chemicals, Busan, Republic of Korea), acetic acid (99.7 %), sulfuric acid (98.08 %), hydrochloric acid (35 %) (mass/mass, Wako Chemicals, Osaka, Japan), 1.5 M Tris-HCl buffer (pH -8.8, Bio-Rad), F-actin probe, and mounting media (Invitrogen, Thermo-Fischer Scientific, USA). The pine wood powders (80 mesh, 177 μm) were used to extract nanocellulose.

2.2. Extraction of spherical nanocellulose (s-NC) and modification with tannic acid (TA)

The spherical nanocellulose (s-NC) was extracted from pine wood powders through chemical treatment. The detailed processes are given in the Supplementary section of the manuscript. The TA functionalized s-NC was prepared as previously reported somewhere else with some modifications [29]. In brief, 1.0 g of s-NC was added to 50 mL of buffer solution and sonicated for 10 min, followed by TA (0.5 g) in the s-NC suspension. The reaction mixture was mechanically stirred for 8 h at room temperature. After that, reaction media were filtered and washed with distilled water. The sample was dialyzed using a cellulose tube (MW: 12–14 kDa) against distilled water for 3 days. The dialyzed sample was freeze-dried using a freeze dryer (EYELA® Freeze Drying Unit 2200, Tokyo, Japan) for 2 days. The obtained sample was indicated by TA@s-NC.

2.3. Preparation of PVA and PVA/tannic acid functionalized nanocellulose (PVA/TA@s-NC) hydrogels

The PVA hydrogel was prepared in distilled water. For this, the calculated amounts of PVA (15 wt%) were added to 30 mL distilled water and heated at 95 °C for 3 h to homogenize the PVA solution. The obtained PVA solution was cross-linked with 0.1 M borax solution. The air bubbles were removed using an ultrasonic bath sonicator. The sample was stored at 4 °C for 12 h, followed by −20 °C for 4 h to obtain a more cross-linked structure. The sample was unfrozen at room temperature for 6 h. The freezing-thawing process was done one time. The PVA/TA@s-NC hydrogels were prepared similarly by incorporating the calculated amounts of TA@s-NC (1, 2, and 4 wt%, w.r.t. to PVA wt.) in PVA solution and cross-linked by 0.1 M borax solution. The s-NC-incorporated PVA hydrogels were also synthesized to examine the effects of s-NC on the mechanical strength of the developed hydrogels. The prepared hydrogels were indicated by PVA, PVA/TA@s-NC-y, and PVA/s-NC-y, where y is the amount of TA@s-NC and s-NC in the PVA polymer. Similarly, the PVA/TA@s-NC 6 hydrogel was also fabricated.

2.4. Characterization

The chemical composition of TA, s-NC, TA@s-NC, PVA, and PVA/TA@s-NC was analyzed using Fourier transform infrared (FTIR) spectroscopy (Frontier, Perkin Elmer, UK) in the wavelength range of 4000–500 with the resolution of 4 cm^{-1}. The number of scans was 64. The mechanical strength of the developed hydrogels was evaluated using the universal testing machine (UTM) (MCT-1150, A&D, Co. Japan) in tensile and compression modes with 10.0 mm/min speed. The viscoelasticity of the hydrogels was analyzed using an ARES-GE rheometer (TA Instrument, New Castle, Delaware, USA) on a 6 mm parallel plate at 25 °C.

2.5. Self-healing and adhesive analysis

The cutting and re-joining method was used to examine the self-healing potential of the hydrogels. Briefly, a fixed dimension of the hydrogel was cut into pieces and contacted to re-join at room temperature without using external stimuli. We have colored one part of the hydrogel with the acridine orange (AO) dye to visualize the self-healing process.

The adhesive strength of the hydrogels was measured by the lap shear method on the paper surface (15 mm × 13 mm) through UTM at room temperature. Hydrogel (100 mg) was spread over the paper surface, covered with another paper, and left for 20 min. The hydrogel was sandwiched between two paper surfaces. All experiments were conducted in triplicate ($n = 3$), and the average data were considered for the

adhesive strength.

2.6. Shape memory analysis

The temperature-induced shape memory behavior of the hydrogels was examined by the cyclic bending test. Briefly, a straight strip of the hydrogel was bent at a given angle (θ_i) and placed in hot water (55 °C) for 10 s. The bent strip was transferred into the cold water (25 °C) for 30 s to achieve the proper deformation (θ_f). The shape fixing ratio (R_f) was calculated by using the following equation,

$$\text{Shape fixing ratio } (R_f) = \frac{\theta_f}{\theta_i} \times 100$$

The de-formed strip was again placed in hot water (55 °C) for 10 s to recover the original structure, followed by the measurement of the residual angle (θ_p). The shape recovery ratio (R_r) was determined by using the following equation,

$$\text{Shape recovey ratio } (R_r) = \frac{\theta_f - \theta_p}{\theta_f} \times 100$$

2.7. Examination of anti-freezing property

The anti-freezing property of the hydrogels was assessed at −20 °C after six days of incubation. For this, the hydrogels were kept at −20 °C for six days, and the change in physical appearance was analyzed. The photographs of the hydrogels were captured after keeping them at room temperature for a few minutes (~3 min) to melt the ice crystals on the surface of the hydrogels. The change in the mechanical strength was also determined through the UTM.

2.8. Cytotoxicity analysis

The biocompatibility of the hydrogels was evaluated with human dermal fibroblasts (HDF) cells through WST-8 assay after 24 h incubation. For this, HDF cells (1.0×10^4) were incubated with or without the hydrogels in a 5 % CO_2 incubator at 37 °C. The media without hydrogels were considered as control. After incubation, the cells were washed with PBS, and WST-8 dye (10 μL) was added to the cultured media and incubated for 2 h to develop formazan. A spectrophotometer (Infinite® M Nano 200 Pro, TECAN, Switzerland) was used to quantify the formed formazan by taking the absorbance at 450 nm. All measurements were done in triplicate ($n = 3$), and the data are presented as mean optical density (OD) ± standard deviations (SDs). Statistical significance was considered as $^*p < 0.05$.

The morphologies of the cultured HDF cells were examined through an inverted fluorescence microscope (DMi8 Series, Leica Microsystems, Germany) after 24 h of incubation. 2.0×10^4 HDF cells were treated with or without the developed hydrogels. The media without hydrogels were taken as control. The cells were rinsed with PBS, followed by cell fixing through a 4 % PFA solution. The PFA-treated cells were washed with PBS and incubated with 0.1 % Triton-X 100 for 10 min. After that, cells were treated with 1 % BSA solution for 1 h, then staining 200 μL of Alexa flor 488-conjugated Phalloidin for 20 min. The nuclei were stained with DAPI for 5 min, followed by washing with PBS to remove the excess stains. After that, 1 drop of Prolong® Antifade mounting media was added, and morphologies were taken with the microscope.

2.9. Antibacterial property

The antibacterial potential of the hydrogels was assessed through agar diffusion assay, as previously reported somewhere [30]. In brief, a few colonies of *Escherichia coli* (*E. coli*) (ATCC 10536) were suspended in the nutrient broth and incubated at 37 °C for 12 h with continuous stirring (200 rpm) to obtain the new bacteria colonies. After that, the optical density (O.D.) of the cultured bacterial was taken at 600 nm using a spectrophotometer, followed by dilution at 10^{-2} from initial concentrations. The diluted bacteria media were placed on agar plates. Approximately equal weights of the hydrogels (0.170 g) were placed on the agar plates and incubated at 37 °C for different periods (36 and 60 h). Each experiment was performed in triplicate ($n = 3$). Furthermore, 100 μL of freshly cultured bacteria solution was added to a nutrient broth having 5 mL of culture media with hydrogels (30 mg/mL) and incubated for 24 h at 37 °C. The media without hydrogel treatment were taken as control. After incubation, 100 μL of the bacteria solution was plated onto agar plates and further incubated at 37 °C to form the colony.

2.10. Electrochemical and sensing analysis

The conductivity of the developed hydrogels was measured using a four-probe instrument (MS Tech, solution) connected with the Keithley 2460 source meter® at room temperature. The hydrogel dimensions and their resistance are mentioned in Table S1. The hydrogel conductivity was calculated by using the equation given below,

$$\text{Conductivity} = \frac{L}{RA}$$

here L, R, and A are the length, resistance, and area of the hydrogels, respectively.

The conductance behavior of the developed hydrogels was determined through the slope of the current-voltage (IV) curve. The dimensions of the hydrogel are given in Table S2. The conductance of the hydrogels was determined by using the following equation,

$$\text{Conductance } \left(\frac{1}{R}\right) = \text{Slope of } \frac{I}{V} \text{ curve}$$

The electrochemical response of the hydrogel was monitored with the Keithley 2460 source meter® at room temperature. The platinum (Pt) disc and silver (Ag/AgCl) served as working and reference electrodes in sulfuric acid solution (1 mol/L), respectively. The 3.0 M potassium chloride solution was used as a supporting electrolyte in cyclic voltammetry work.

The sensing abilities of the hydrogels (fresh, healed, and freeze conditions) were also assessed with the Keithley 2460 source meter® at 5 V. The change in the current with time was recorded and analyzed. The relative resistance change ($\Delta R/R_0$) was determined by using the following equation,

$$\text{Relative resistance change } \left(\frac{\Delta R}{R_0}\right) = \frac{(R_s - R_0)}{R_0} \times 100$$

where, R_0 and R_s are the resistance of hydrogel before and after strain, respectively.

The strain sensitivity of the hydrogel was determined by gauge factor (GF), which was calculated by using the following equation,

$$\text{Gauge factor (GF)} = \frac{\left(\frac{\Delta R}{R_0}\right)}{\varepsilon}$$

here $\left(\frac{\Delta R}{R_0}\right)$ and ε are the relative resistance change and applied strain, respectively.

2.11. Statistical analysis

Statistical analyses were accomplished with one-way ANOVA using Origin Pro9.0 software. All results are shown as mean ± standard deviations (SD). Statistical significance was taken at $^*p < 0.05$, $^{**}p < 0.01$, and $^{***}p < 0.001$. The comparison was performed between the control and experimental groups.

3. Results and discussion

3.1. Surface functionalization of s-NC and the mechanical strength of the hydrogel

A schematic presentation for synthesizing of the hydrogels and their possible applications in sensing is shown in Scheme 1. The transmission electron microscopy (TEM) image of the pine wood-derived s-NCs is shown in Fig. S1a. The extracted s-NCs had a nearly spherical structure with an average diameter of ~43 nm. The photographs of pure s-NC and TA@s-NC suspensions are shown in Fig. S1b. A homogenous suspension was observed in the aqueous medium, indicating the fine dispersion and enhanced stability of the materials. The Fourier-transform infrared (FTIR) spectra of the pure TA, s-NC and TA@s-NC are shown in Fig. 1a.

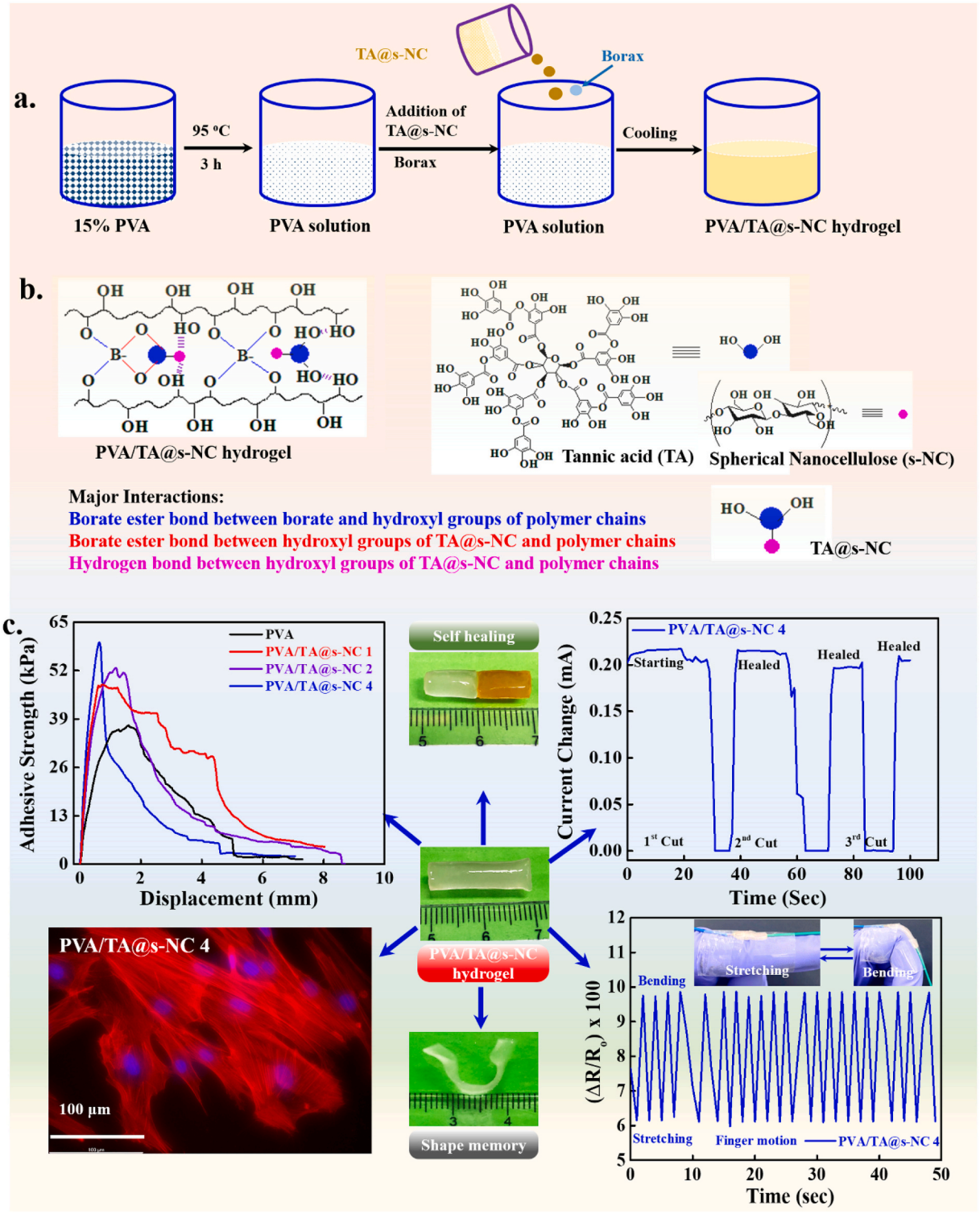

Scheme 1. (a) The schematic presentation for the synthesis of multifunctional polyvinyl alcohol/tannic acid functionalized spherical nanocellulose (PVA/TA@s-NC), (b) major possible interactions within the developed hydrogels with chemical structure of TA, and s-NC, and (c) different desired properties of the developed hydrogels for sensing applications.

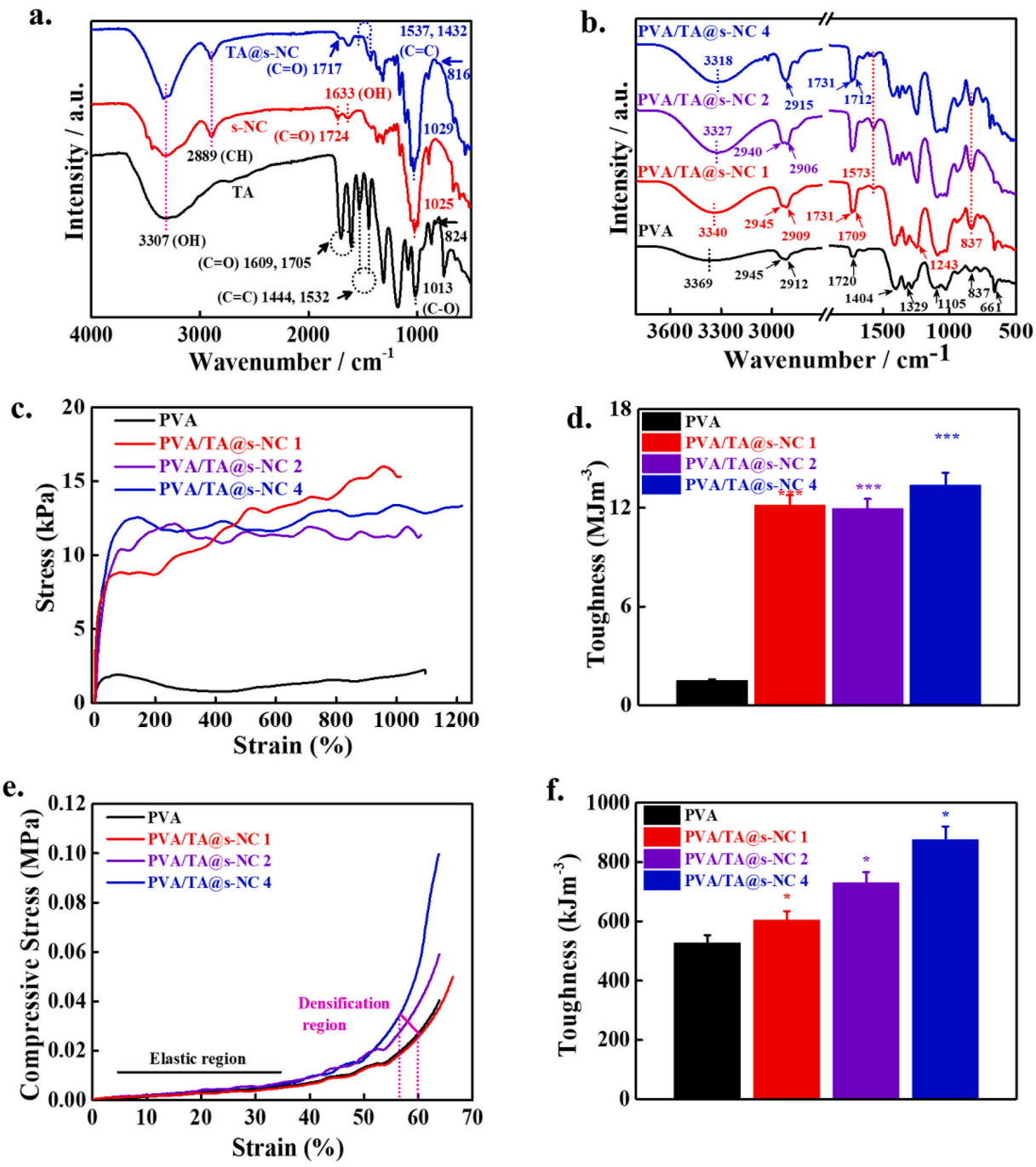

Fig. 1. The spectroscopic characterization of TA@s-NC and mechanical strength of the developed hydrogels. (a) FTIR spectra of the pure TA, s-NC, and TA@s-NC, (b) FTIR spectra of the developed hydrogels, (c) stress-strain curves of the developed hydrogels under tensile condition, (d) toughness value of the indicated hydrogels, (e) stress-strain curves of the developed hydrogels under compressive condition, and (f) toughness value of the indicated hydrogels.

The characteristic absorption peaks at 3307, 1705–1609, 1532–1444, 1013, and 824 cm^{-1} in TA were assigned to the –OH stretching vibration, C═O, C═C (aromatic stretching), C—O vibration, and C═C (aromatic bending) vibration, respectively [31,32]. The absorption peaks at 3307, 2889, 1724, 1633, and 1025 cm^{-1} in pure s-NC can be attributed to –OH stretching, $–CH_2$ stretching, –C═O, absorbed water, and C—O vibration, respectively. Notably, no absorption peaks occurred in the 1500 cm^{-1} region in pure s-NC, suggesting the complete removal of the non-cellulosic components (lignin) through chemical treatment. The absorption peaks at 2889, 1717, 1532, 1432, and 816 cm^{-1} in TA@s-NC demonstrated the successful functionalization of TA with s-NC in an aqueous medium. Moreover, the –OH stretching peak of TA@s-NC became narrow than the pure TA, suggesting strong interactions between TA and s-NC. PVA/TA@s-NC hydrogels were prepared by incorporating the appropriate amounts of TA@s-NC in an aqueous medium of PVA polymer at 90 °C. The FTIR spectra of the pure PVA and PVA/TA@s-NC hydrogels are shown in Fig. 1b. The characteristic absorption peaks of PVA hydrogel at 3369, 2945–2912, 1720, 1329, 1109, 837, and 661 cm^{-1} are assigned to OH stretching, CH_2 asymmetric stretching vibration, C═O stretching, CH_2 bending vibration, C—O stretching of acetyl groups, C—C stretching vibration, and OH wagging vibration, respectively [33]. A significant shift in OH stretching peak observed in the composite hydrogels (3369 → 3318 cm^{-1}) is attributed to the strong interactions (hydrogen and ester bonding) between polymer chains and

TA@s-NC. The composite hydrogels exhibited intense CH_2 asymmetric stretching vibration peaks compared to the pure polymer due to the incorporated TA@s-NC. The absorption peak at 1731 cm^{-1} indicates the presence of TA@s-NC moieties. Shifting in the absorption peak of C═O groups (1720 → 1709 cm^{-1}) was observed in the composite hydrogels due to the interactions between the polymer chains and added nanomaterial. The composite hydrogels also show a prominent absorption peak at 837 cm^{-1}, which overlapped the C—C stretching vibration of polymer chains. These results suggest that the developed hydrogels were interactive, and hydrogen, as well as borate ester bonds play significant roles in these shifting [34].

Before examining the effects of TA@s-NC on the mechanical strength of the PVA hydrogel, we measured the mechanical strength of s-NC-added PVA hydrogels by UTM in tensile mode, and the results are shown in Fig. S2a–b. The s-NC-incorporated hydrogels exhibit enhanced mechanical strength (ultimate strength and toughness) compared to the pure PVA hydrogel, demonstrating its reinforcing effects. However, this enhancement was lower than the TA@s-NC-added hydrogel, suggesting that functionalization positively affects mechanical strength. A decrease in the mechanical strength of nanocellulose-based composites has been previously reported because of poor interfacial compatibility and interaction between nanocellulose and the polymer matrix [35]. The stress-strain curves of the developed hydrogels are shown in Fig. 1c. The TA@s-NC-added hydrogels show enhanced ultimate strength compared to the pure polymer hydrogel, indicating the reinforcing effects of the added TA@s-NC. Approximately 6 times (2.21 kPa → 13.25 kPa) enhancement in the ultimate strength was observed in the composite hydrogels than in the pure polymer. This enhancement was attributed to the different interactions, including hydrogen bonding, ester bonding, and π-bonding between the TA@s-NC and PVA chains, which facilitated the load transformation during elongation [36]. As the TA@s-NC content increased, a systematic enhancement in the elongation at break was observed, indicating that the addition of TA@s-NC significantly enhanced the toughness and stretchability of the PVA hydrogel. An enhancement in the elongation at break is explained by the suppression of the crack propagation process by added nanomaterial through the effective interactions (hydrogen bonding, ester bonding, and π-bonding), causing a higher elongation at break. More significant suppression of the crack propagation process occurred at a high content of TA@s-NC, leading the superior elongation at break [37]. The developed hydrogels exhibited greater elongation at break properties than previously reported PVA hydrogels, and value is mentioned in Table 1 [22,38–42]. The Young's modulus value (from the slope of the initial stress-strain curves) was 0.037 ± 0.012, 0.134 ± 0.005, 0.238 ± 0.007, and 0.24 ± 0.006 kPa for PVA, PVA/TA@s-NC 1, PVA/TA@s-NC 2, and PVA/TA@s-NC 4, respectively. Approximately 6.5 times enhancement in Young's modulus was observed the in composite hydrogels than in the pure polymer, showing the improved elasticity in the composite hydrogels due to the better interaction. The toughness was calculated from the stress-strain curve (area under the curve), and the results are shown in Fig. 1d. The composite hydrogels show improved toughness value compared to the pure polymer hydrogel. Approximately 8.9 folds (1.5 MJ m^{-3} → 13.39 MJ m^{-3}) enhancement in the toughness was observed in the composite hydrogels than the pure polymer hydrogel. This improvement was attributed to the inhibition of the crack propagation process by TA@s-NC during measurement.

Table 1
A comparative analysis of the elongation at break of previously reported PVA-based hydrogels with this study.

Components	Elongation at break (%)	References
Polyvinyl alcohol/cellulose nanofiber/aluminum chloride hexahydrate	696	[38]
Polyvinyl alcohol/cellulose nanofibrils	660	[39]
Polyvinyl alcohol/gelatin/cellulose nanocrystal	82	[40]
Polyvinyl alcohol/nanocellulose	600	[41]
Polyvinyl alcohol/polypyrrole/cellulose nanofibers	820	[22]
Polyvinyl alcohol/tannic acid/ carboxymethylated cellulose nanofibrils/ sulfonated carbon nanotubes	300	[42]
Polyvinyl alcohol/tannic acid/nanocellulose	1211	This study

The mechanical strength of the materials is profoundly affected by the crosslinking density, polymer concentration, molecular weight, surrounding conditions (pH, temperature, solvent, and loading rates), and physicochemical properties of the added nanomaterials [43]. We further measured the mechanical strength of the hydrogel at a higher content of TA@s-NC (6 wt%) to examine the reinforcing effects of the added nanomaterial, and the obtained stress-strain curve is given in Fig. S3a. PVA/TA@s-NC 6 hydrogel exhibits a lower ultimate tensile strength than PVA/TA@s-NC 4 hydrogel. It was 6.21 kPa, and 13.25 kPa for PVA/TA@s-NC 6, and PVA/TA@s-NC 4 hydrogels, respectively. The agglomeration of the nanomaterial at a higher concentration caused a decrease in tensile strength [37]. The ultimate tensile strength and toughness value of PVA/TA@s-NC 6 hydrogel is shown in Fig. S3b. A decrease in the toughness was also observed in PVA/TA@s-NC 6 hydrogel (10.5 MJ m^{-3}) compared to PVA/TA@s-NC 4 hydrogel (13.39 MJ m^{-3}). Minimizing the interactions within hydrogel components is the primary factor for decreasing the toughness. These findings suggest that 4 wt% of TA@s-NC are appropriated amounts to enhance the mechanical strength of PVA/TA@s-NC hydrogels.

The images of the stretched hydrogels are presented in Fig. S4. The hydrogel shows high stretchability. The quantitative elongation value is given in Fig. S5. It was 1091.7, 1080.8, and 1211.3 % for PVA, PVA/TA@s-NC 2, and PVA/TA@s-NC 4, respectively. Materials with high stretchability and flexibility are suitable for wearable electronic devices. It can be directly combined with textiles to develop wearable human-machine interfaces for different applications. We further examined the structural moldability potential of the hydrogel, and the images of the hydrogel under different deformation conditions are shown in Fig. S6. These results indicate that the developed hydrogel can be configured in the desired structures without breaking its shape. Moldability enables the development of flexible wearable electronic devices where complex configurations are required [44].

Further, the mechanical strength of the hydrogels was also measured in compressive mode, and the obtained stress-strain curves are presented in Fig. 1e. We compressed the hydrogels up to ~63 % of their original height at a compression rate of 10 mm/min. The hydrogel exhibits the properties of a typical porous material with a linear elastic region at relatively low stress, followed by a plateau and densification region. An enhancement in the compressive strength (0.040 MPa → 0.099 MPa) was observed in the composite hydrogels than in pure PVA hydrogel due to the greater load transfer in the presence of TA@s-NC during compression. Graphene oxide-added PVA hydrogels exhibited enhanced compressive strength than pure PVA hydrogels owing to the strong interaction between the PVA and graphene oxide, which transferred the load from the polymer chains to the graphene oxide [45]. The toughness value of the developed hydrogels under compressive mode is shown in Fig. 1f. The composite hydrogels demonstrate enhanced toughness compared to the pure PVA hydrogel. The toughness enhancement was attributed to the barrier effects of the TA@s-NC in the polymer matrix, which restricted the crack propagation process during compression. Furthermore, the composite hydrogels demonstrated a lower densification value than the pure polymer hydrogels, suggesting a more cross-linked structure. These results indicated that added TA@s-NC improved the mechanical strength of the PVA hydrogel.

3.2. Viscoelasticity and recovery analysis

The viscoelasticity of the developed hydrogels was determined using a rheometer in the measured region of 0.1–100 rad/s at 25 °C, and the results are shown in Fig. 2a. No crossover of the storage modulus (G′,

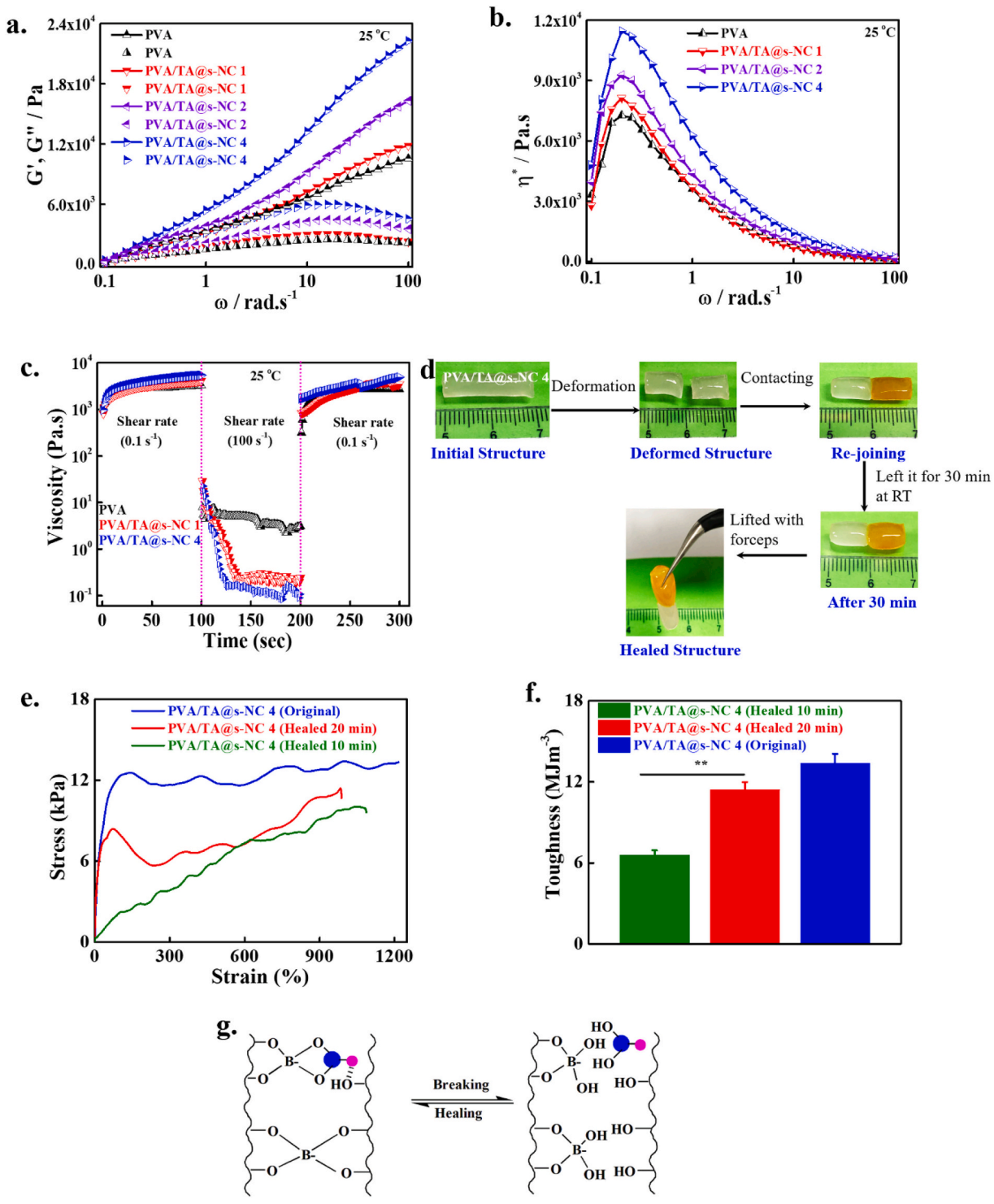

Fig. 2. Analysis of viscoelasticity of the developed hydrogels at indicated temperature. (a) Storage modulus (G′, continuous line) and loss modulus (G″, without line) of the developed hydrogels in the measured regions, (b) change in viscosity complex of the developed hydrogels in the measured regions, (c) change in the viscosity of the developed hydrogels w.r.t. the shear rates at indicated time periods, (d) examination of self-healing efficiency of the developed hydrogel at room temperature in the absence of external stimuli (temperature, pressure, and pH), (e) stress-strain curve of the original and healed PVA/TA@s-NC 4 hydrogels, (f) toughness values of the original and healed PVA/TA@s-NC 4 hydrogels, and (g) the possible mechanism for breaking and self-healing process in the indicated hydrogels.

solid lines) and loss modulus (G″, without lines) was observed in the measured regions, suggesting typical solid-like properties. The composite hydrogels show a higher G′ value than the pure PVA hydrogel over the entire measurement regions and increase with increasing TA@s-NC content in the polymer matrix. The improvement in the G′ value of the composite hydrogels is attributed to the formation of strong polymeric networks, leading to improved elasticity of the hydrogels. Different kinds of interactions, such as borate ester between the PVA chains and borax, borate ester between the PVA chains and the vicinal hydroxyl groups of TA@s-NC, π–π interactions, and hydrogen bonding between the PVA chains and TA@s-NC, are responsible for the elasticity enhancement of the hydrogels [46]. An enhancement in the G′ of the

PVA hydrogels with CNFs was previously reported due to the formation of cross-linked polymeric structures [47]. A significant enhancement in the G′ value of the composite hydrogels (1.05×10^4 Pa → 2.22×10^4 Pa) has occurred at a higher angular frequency (100 rad/s) than that of the pure PVA hydrogel, indicating their improved elasticity. The improvement in the G′ value of the composite hydrogels at high angular frequency is due to the relaxation and simultaneous formation of more interconnected polymeric network structures within the hydrogel components, which restricts the movement of the polymer chains, resulting in a solid-like property and higher G′ value [48,49]. The composite hydrogels exhibited a higher G″ value than the pure polymer throughout the measured regions. However, their magnitudes were lower than those of G′ over the entire measured regions, indicating the existence of stable crosslinked polymeric networks in the hydrogels. The corresponding complex viscosity (η*) values of the hydrogels in the measured regions are shown in Fig. 2b. The composite hydrogels exhibit higher η* values than the pure polymer, suggesting the existence of solid-like structures. This value increased with increasing TA@s-NC content in the polymer matrix due to more cross-linked networks.

Furthermore, the hydrogels demonstrate a higher η* value at a low angular frequency. In contrast, a decreased η* value was observed at a relatively high angular frequency, showing shear thickening and thinning properties of the hydrogels. The shear thickening phenomenon in the developed hydrogels is attributed to forming compact solid-like structures *via* different interactions between the polymer chains, nanomaterial and the crosslinking agent. These interactions led to the proper entanglement of the randomly oriented polymer chains at a lower angular frequency. The shear thinning behavior in the developed hydrogels at a higher angular frequency is assigned for the disentanglement of the polymer chains, which led to reduced interactions between the added components, and decreasing viscosity [28,50].

Recoverable hydrogels have attracted significant interest in developing wearable electronic devices owing to their recovery potential after deformation. The recovery potential of the developed hydrogels was analyzed by measuring the viscosity (η) at different shear rates (0.1, 100, and 0.1 s^{-1}) for 100 s at 25 °C, and the results are shown in Fig. 2c. The η value was 3247.0, 4103.4, and 5374.6 Pa·s for PVA, PVA/TA@s-NC 1, and PVA/TA@s-NC 4 hydrogels at a low shear rate (0.1 s^{-1}), respectively. These values decreased to 3.0, 0.2, and 0.1 Pa·s for PVA, PVA/TA@s-NC 1, and PVA/TA@s-NC 4 hydrogels, respectively, at a high shear rate (100 s^{-1}). The high shear rate (100 s^{-1}) deformed the crosslinked networks in the hydrogels, leading to a lower η value. The hydrogels recovered approximately the initial η values after removing the high shear rate, and it was 2653.3, 3452.4, and 4870.2 Pa·s for PVA, PVA/TA@s-NC 1, and PVA/TA@s-NC 4 hydrogels, respectively. The recovery values were 81.62 %, 84.13 %, and 90.61 % for PVA, PVA/TA@s-NC 1, and PVA/TA@s-NC 4 hydrogels, respectively. The composite hydrogels demonstrated improved recovery strength compared to the pure polymer, which increased with increasing TA@s-NC content in the polymer matrix. The higher recovery strength of the composite hydrogels was due to the formation of more cross-linked structures in the hydrogels. A high recovery strength in PVA/starch hydrogels has been previously reported because of the formation of cross-linked polymeric networks [51].

Self-healed hydrogels with adequate mechanical strength have paid significant attention in fabricating wearable electronic devices and biomedical research. Self-healed hydrogels have more prolonged durability than typical hydrogels [52]. The macroscopic self-healing potential of the developed hydrogel was analyzed using the cut-and-re-joining method at room temperature, and the results are shown in Fig. 2d. The separated hydrogels were ultimately rejoined within 30 min without using any external stimuli, showing their self-healing ability. The relatively high self-healing ability of the hydrogel was attributed to the reversible borate ester linkages, π–π bonding, and hydrogen bonding between the hydrogel components. Hydrogels based on nanoclays and hydrophilic monomers have been extensively explored to develop stretchable and self-healing materials for various applications [53]. Different molecular interactions, including hydrogen and covalent bonding, ionic interactions, hydrophobic interactions, metal-ligand coordination, and host-guest interactions, play significant roles in the self-healing ability of the materials [54]. We further analyzed the mechanical strength of the original and healed PVA/TA@s-NC 4 hydrogels to assess their self-healing efficiency. The stress-strain curves of the original and healed hydrogels are shown in Fig. 2e. The healed hydrogels recovered their mechanical strength and elongation at break to the original hydrogel with increasing the healing time, suggesting the effective self-healing ability of the hydrogel. The quantitative toughness values of the original and healed hydrogels at different intervals (10 and 20 min) are shown in Fig. 2f. The toughness values were 6.6, 11.41, and 13.39 MJ m^{-3} for 10 min healed hydrogel, 20 min healed hydrogel, and original hydrogels, respectively. The toughness value was approximately 49.3 % and 85.2 % of the original hydrogel after 10 and 20 min of the self-healing process. The self-healing efficiency of the hydrogel might be further increased by increasing the healing time owing to the relatively high crosslinks among the hydrogel components [55]. The photographs of the healed hydrogel during the mechanical analysis are shown in Fig. S7. The healed hydrogel exhibited elongation properties similar to the original hydrogel without breaking at the healing point. A possible mechanism for the improved self-healing ability of the developed hydrogel is presented in Fig. 2g. Different borate ester linkages, π–π bonding, and hydrogen bonding are reversible and easily dissociated during breaking and readily re-associated after contact. The hydrogels with autonomous healing ability are attractive platforms for fabricating wearable electronic devices because of their rapid dissociation and association ability, and they can be modulated by external stimuli [56].

3.3. Adhesive behavior of hydrogel

Self-healing hydrogels with adequate adhesiveness are highly desired to develop strain sensors due to the non-requirement of external adhesive tapes or bandages, which may cause skin irritation for long-term measurements. The adhesiveness of the hydrogels was monitored with different surfaces. The photographs of the developed hydrogel with human skin, Eppendorf tube, rubber, and centrifuge tubes are given in Fig. 3a(i–iv). The hydrogel was adequately adhered to different surfaces, demonstrating its adhesiveness. The quantitative adhesive strength of the hydrogels was measured through UTM with thick paper surfaces. The load *vs.* displacement curves for the developed hydrogels are shown in Fig. 3b. The composite hydrogels exhibit higher load-bearing capacity than the pure polymer, suggesting their better strength. This potential was further increased with increasing TA@s-NC in the polymer matrix, showing the improved load-bearing strength of composite hydrogels.

The improved load-bearing strength of the composite hydrogels can be attributed to the more significant interactions between the hydrogel components and the applied surface. The presence of active functional groups in the composite hydrogels facilitated greater interactions. The adhesive strength *vs.* displacement curves for the developed hydrogels are given in Fig. 3c. The composite hydrogels show greater adhesiveness than the pure polymer hydrogel, indicating their superior adhesive strength. The adhesive potential of the hydrogels is profoundly affected by the physicochemical properties of hydrogels, adhesion time, and surface properties of applied materials [57]. The quantitative values of the adhesive strength with paper surfaces are given in Fig. 3d. The adhesive strength was 37.07 ± 1.85, 48.05 ± 2.40, 52.63 ± 2.63, and 59.64 ± 2.98 kPa for PVA, PVA/TA@s-NC1, PVA/TA@s-NC 2, and PVA/TA@s-NC 4, respectively. The adhesive strength of the fabricated hydrogels may increase with polar surfaces, including human skin, due to the presence of the charged functional groups, which cause better interactions. The possible interaction mechanism between the applied paper and the developed hydrogels is presented in Fig. 3e. The paper is composed of cellulose, which has an abundance –OH groups in their compositions. The hydrogels have abundant active hydroxyl groups in

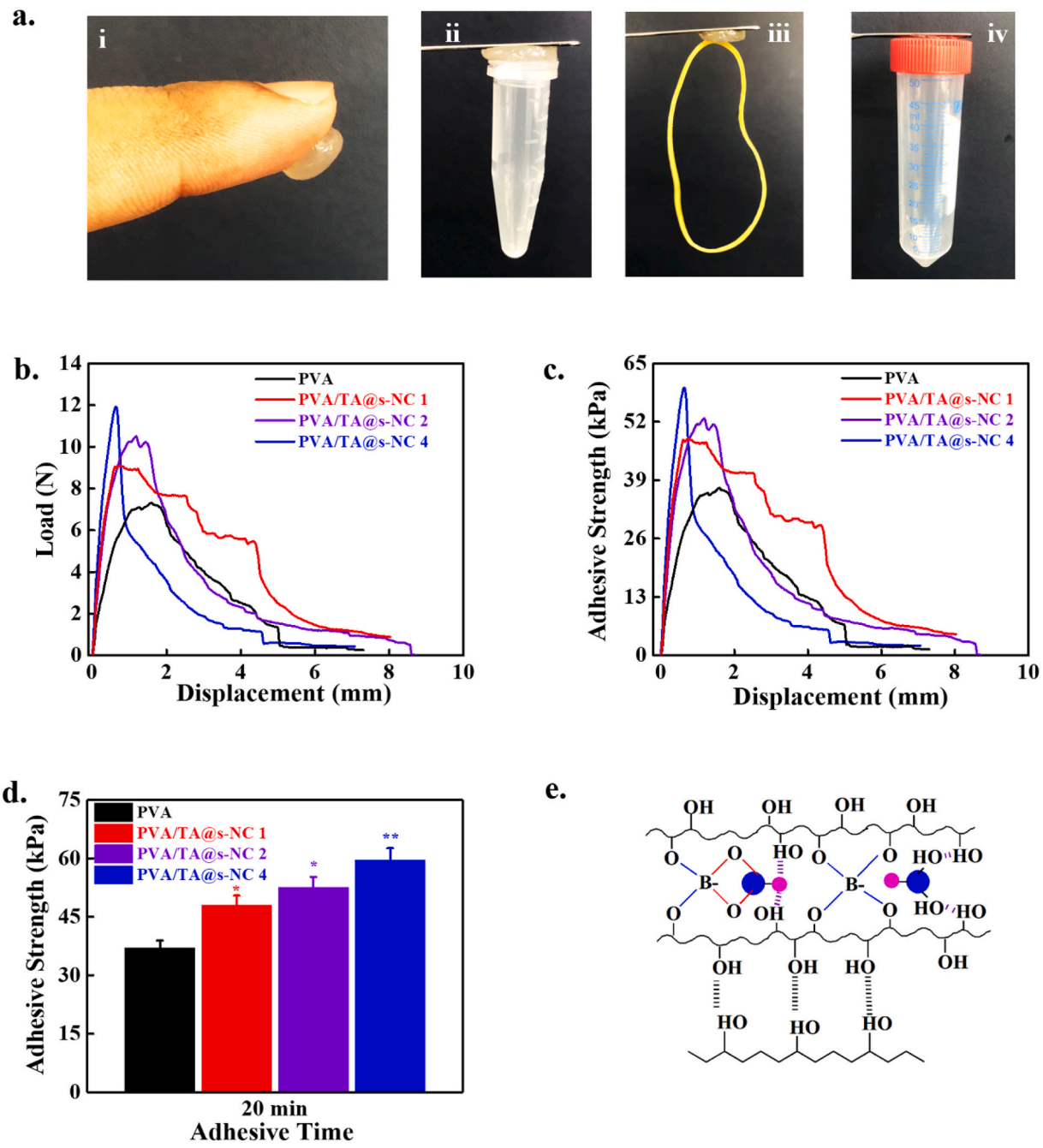

Fig. 3. (a) Examination of the adhesiveness of the developed hydrogels at different surfaces (i) human skin, (ii) Eppendorf tube, (iii) rubber, and (iv) centrifuge tube, (b) load *vs.* elongation curves of the indicated hydrogels sandwich between two paper surfaces, (c) adhesive strength (kPa) *vs.* displacement curves of the indicated hydrogels, (d) quantitative values of the adhesive strength of the developed hydrogels after 20 min of treatment sandwich between two plastic surfaces, and (e) the possible mechanism for interaction between paper surface and hydrogel.

their structures, which strongly interact with cellulose chains through different approaches, including hydrogen bonding, dipole-dipole, or ion-dipole interactions. The possible interactions between different functional groups (–C═O and –S═O) and the developed hydrogels are (Fig. S8). Zhao et al. have also reported the superior adhesive potential of fibroin-based hydrogels with different surfaces, including human fingers, glass, rubber, and plastic, through different interactions, such as hydrogen bonding, electrostatic and hydrophobic interactions [58].

3.4. Shape memory behavior

We performed the shape memory behavior of the PVA hydrogels in a strip form at different heating periods (10, 20, and 30 s) and 55 °C with a fixed cooling time (30 s) to know the optimum time for shape memory behavior, and the images are shown in Fig. S8. The results indicate that a heating time of 10 s for deformation and reformation is appropriate for shape-memory analysis. Therefore, we chose a shape-memory examination time of 10 s. The shape-memory behavior of the developed hydrogels was examined using the shape fixation ratio (R_f) and shape recovery ratio (R_r) at 55 °C; the results are shown in Fig. 4a. The developed hydrogels easily deformed in the desired structure (U-shaped) at 55 °C and maintained their morphologies (temporary shape at 25 °C), showing their shape-fixing ability. The temporary structures were recovered to their original structure within 10 s after applying an

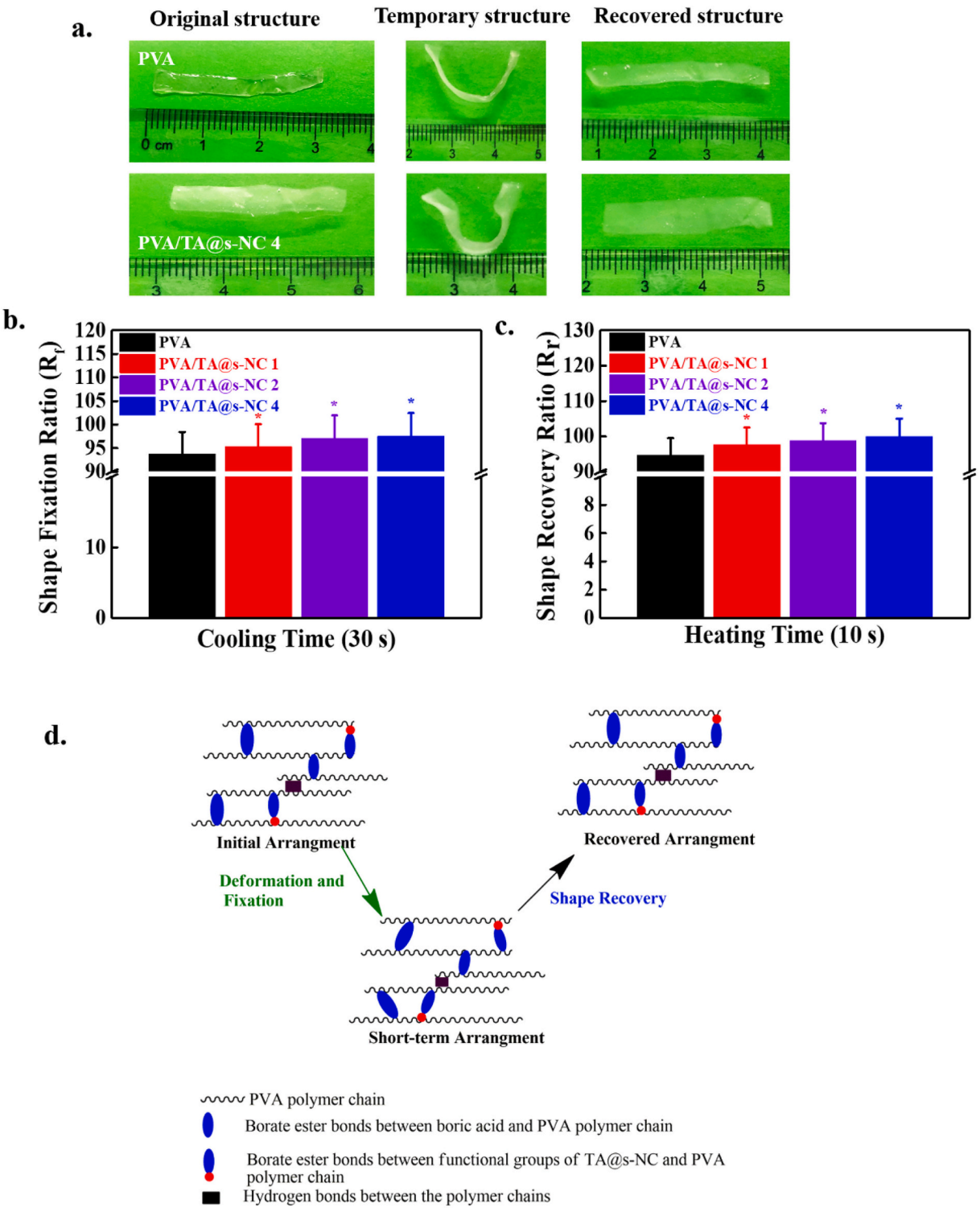

Fig. 4. Evaluation of the shape-memory potential of the developed hydrogel. (a) Change in the shape of the indicated hydrogels during shape memory examination, (b) quantitative value for shape fixation ratio (R_f) of the indicated hydrogels, (c) quantitative value for shape recovery ratio (R_r) of the indicated hydrogels, and (d) the possible mechanism for shape deformation and recovery.

external stimulus (55 °C), demonstrating their shape-recovery potential. The shape-fixing ability of the developed hydrogels was attributed to the minor destruction of the crosslinked structures (predominantly H-bonding) of the hydrogels at a relatively high temperature and immediate cross-linking at low temperatures, leading to shape-fixing potential [59,60]. The composite hydrogels exhibit a better shape-fixing ability than the pure polymer hydrogel because of the increased number of cross-linked structures, as observed in the rheological analysis. The cross-linked structures were significantly damaged in the composite hydrogels at relatively high temperatures, which instantly cross-linked at low temperatures, causing enhanced shape fixation. The shape-fixing ability increased with the increase in the TA@s-NC content in the polymer matrix. Here, we show the images of pure PVA and PVA/TA@s-NC 4 hydrogels for visualization. The deformed hydrogels

recovered their original structures, demonstrating their shape-recovery potential. The composite hydrogels showed improved shape-recovery potential compared to the pure polymer hydrogels and increased with the increase in the TA@s-NC content in the polymer matrix. The improved shape-recovery potential was attributed to the better reformation of hydrogen bonds in the composite hydrogels than in the pure polymer hydrogels. The quantitative values of R_f of the developed hydrogels are shown in Fig. 4b. The values were 93.75 %, 95.32 %, 97.08 %, and 97.56 % for PVA, PVA/TA@s-NC 1, PVA/TA@s-NC 2, and PVA/TA@s-NC 4, respectively.

The high R_f value of the composite hydrogels was attributed to the relatively high destruction and reorganization of the hydrogen bonds in their cross-linked structures. Chen et al. examined the shape-fixing ability of PVA/TA hydrogels [61]. However, their shape-fixing ability was lower than that of our findings. It is likely due to the functionalization of TA with s-NC, providing more functional groups for the destruction and reorganization of hydrogen bonds. The quantitative values of R_r for the prepared hydrogels are shown in Fig. 4c. The values were 94.75 %, 97.61 %, 98.78 %, and 100 % for PVA, PVA/TA@s-NC 1, PVA/TA@s-NC 2, and PVA/TA@s-NC 4, respectively. The relatively high R_r value of the composite hydrogels was significantly due to the reformation of hydrogen bonds. These results indicate that the developed hydrogels have excellent shape-memory abilities and can be explored in sensing and soft robotics. A possible mechanism for the shape memory phenomenon in the developed hydrogels is demonstrated in Fig. 4d. The movement in the polymer chains causes the de-localization of the different interactions in the developed hydrogels during the heating and cooling processes, leading to the formation of a temporary cross-linked structure. The polymer chains regain their initial configuration through heat treatment, facilitating recovery.

3.5. Anti-freezing property

The anti-freezing potential of the hydrogels was monitored after six days of storage at −20 °C. The images of the hydrogels before and after storage are shown in Fig. 5a. No significant change in the physical appearance was observed after six days of storage, suggesting that the hydrogels maintained their structural integrity under harsh conditions. Conductive hydrogels retaining moisture under harsh conditions are favorable for strain-sensing applications in tropical and cold regions. We measured the mechanical strength (compressive mode) of the frozen hydrogels through UTM, and the obtained stress-strain curves are shown in Fig. 5b. The composite hydrogels show higher mechanical strength than pure polymer hydrogel and increase with increasing TA@s-NC content in the polymer matrix. This enhancement in the mechanical strength was due to the formation of more crosslinked structures, which prohibit excess water evaporation [62]. It was 0.0074, 0.0078, 0.0100, and 0.0103 MPa for PVA, PVA/TA@s-NC 1, PVA/TA@s-NC 2, and PVA/

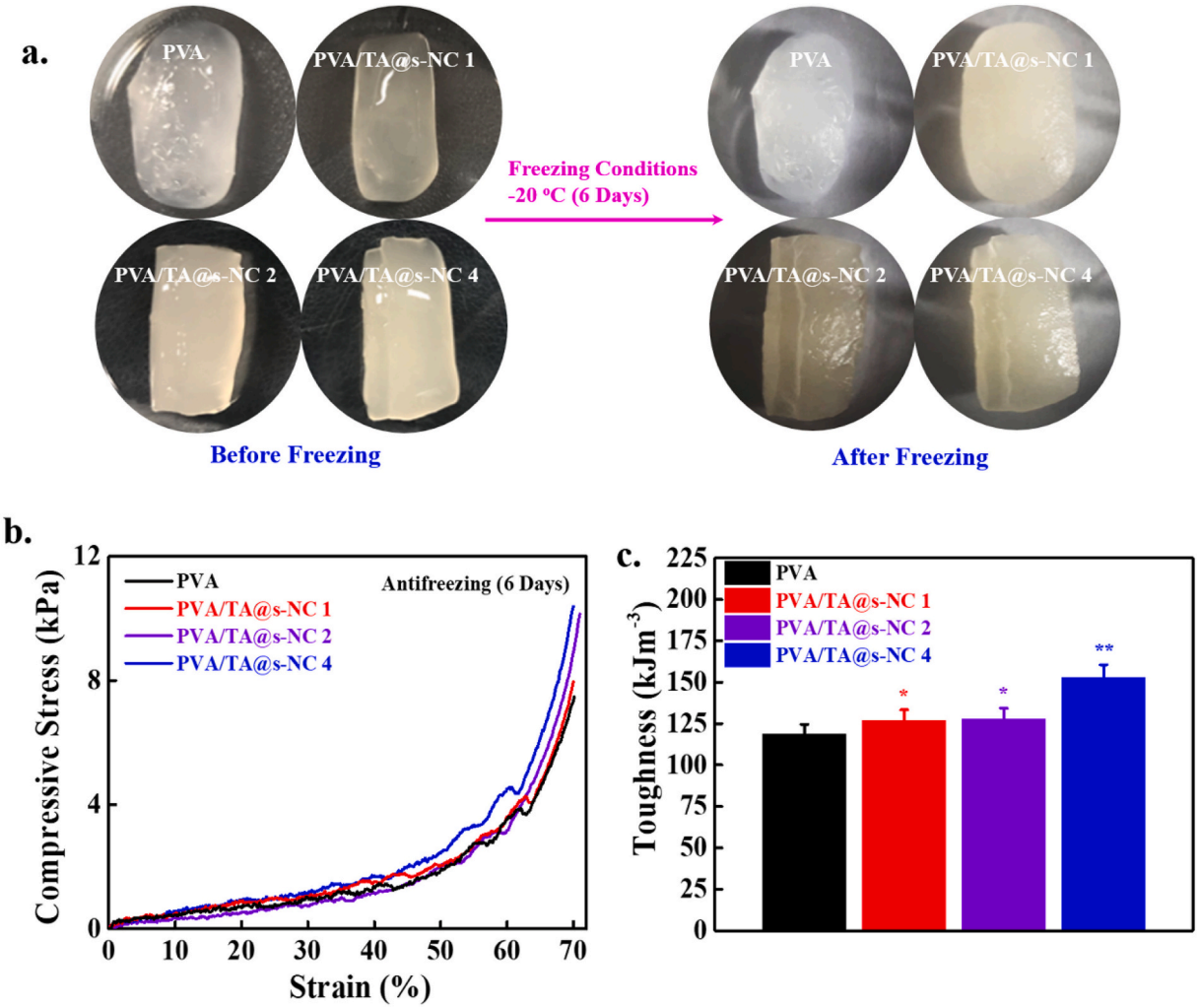

Fig. 5. Examination of the anti-freezing efficiency of the developed hydrogels after 6 days of incubation at −20 °C. (a) The images of the developed hydrogels before and after treatment, (b) stress-strain curves of indicated hydrogels after 6 days of incubation at −20 °C, and (c) quantitative toughness value of the developed hydrogels.

TA@s-NC 4 hydrogels, respectively. These values were lower than in normal conditions, as shown in Fig. 1e. However, the developed hydrogels retained adequate mechanical strength under harsh conditions and exhibited anti-freezing properties. The depressing of the hydrogel freezing point is a significant factor for the anti-freezing potential. The plenty of hydrophilic hydroxyl groups in the hydrogels could hinder the aggregation of water molecules and inhibit the formation of ice crystals, lowering the hydrogels' freezing point. Hydrogen bonding between the polar groups of the hydrogel and water molecules probably plays a crucial role in lowering the freezing point of the hydrogels. The anti-freezing properties of the hydrogels can be further improved by adding freezing resistance media, such as glycerol and ethylene glycol, during the preparation of the hydrogel [63]. Furthermore, we calculated the toughness value of the frozen hydrogels from the stress-strain curves (area under the curve), and the results are shown in Fig. 5c. The toughness values were 118.6, 127.0, 127.9, and 152.9 kPa for PVA, PVA/TA@s-NC 1, PVA/TA@s-NC 2, and PVA/TA@s-NC 4 hydrogels, respectively. The composite hydrogels exhibit enhanced toughness value compared to the pure polymer hydrogel, which is attributed to the inhibition of the crack propagation process through TA@s-NC during the measurement. However, this value was lower than that of normal conditions.

3.6. Cytotoxicity and antibacterial analysis

Biocompatibility of the material is necessary to develop wearable electronic devices for personalized healthcare applications. The cytotoxicity of the developed hydrogels was monitored with HDF cells through WST-8 assay after 24 h of incubation, and the results are shown in Fig. 6a. The groups without hydrogel treatment were considered as controls. The developed hydrogels exhibit no adverse effects on the viability of HDFs, showing their biocompatibility. The composite hydrogel-treated groups show higher cell viability than pure polymer hydrogel, suggesting improved biocompatibility. The cytotoxicity of the developed hydrogels was significantly affected by the TA@s-NC content of the polymer matrix. The improved biocompatibility of the composite hydrogels was attributed to the accelerating effects of biocompatible TA@s-NC in the polymer matrix [64]. The morphologies of the cultured cells after one day of treatment are shown in Fig. 6b. The groups without hydrogel treatment were used as controls. The cells were elongated and in healthy conditions, demonstrating the biocompatibility of the hydrogels.

E. coli bacterium was used as a model bacterium to investigate the antibacterial potential of the developed hydrogels, and the results are shown in Fig. 6c. The experimental areas without any hydrogel treatment were considered as controls. Few bacterial colonies were observed on the surface of the pure PVA hydrogels, whereas no such visualization was observed on the surface of the composite hydrogels after 36 h of incubation, suggesting their improved antibacterial potential. Furthermore, no bacterial growth was observed on the surface of the composite hydrogels after 60 h of incubation, indicating antibacterial efficiency.

The improved antibacterial potential of the composite hydrogels is

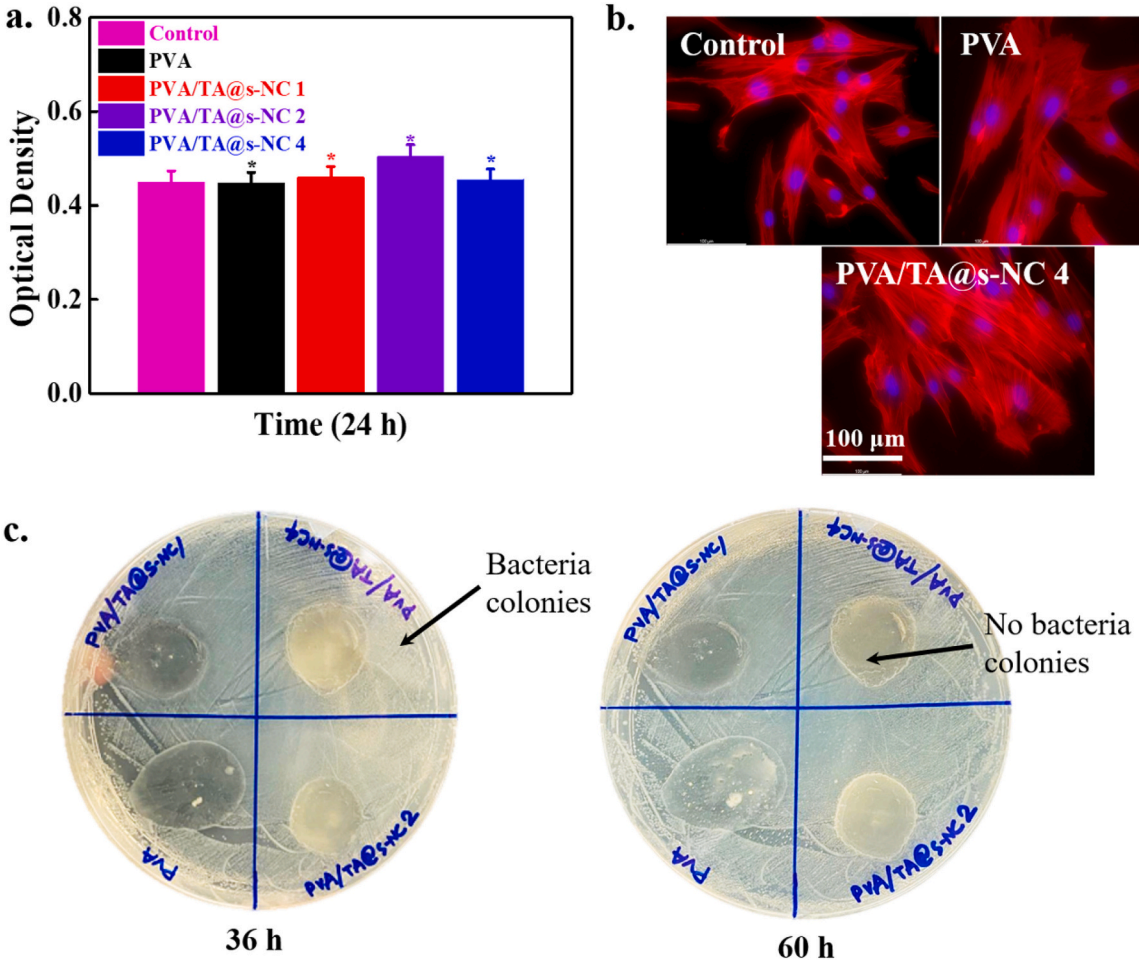

Fig. 6. Evaluation of the biocompatibility and antibacterial potentials of the developed hydrogels. (a) Viability of HDFs cells in with developed hydrogels at indicated time periods, and (b) fluorescence microscopic images of HDFs cells with developed hydrogels after 1 day of treatment, and (c) antibacterial potential of the developed hydrogels at different periods (36 and 60 h).

attributed to the functionalized TA@s-NC in the polymer matrix. The antibacterial activity of TA has been previously reported [26]. Conductive hydrogels with antibacterial potential have significant advantages in developing wearable electronic devices for different applications. These hydrogels remarkably suppressed bacterial infections during human skin contact [65]. We also examined the antibacterial potential of the hydrogels through the agar diffusion method after 72 h of incubation, and the results are shown in Fig. S10. The control and PVA-treated groups contained approximately 821 ± 13 and 708 ± 15 bacteria colonies, whereas PVA/TA@s-NC 4 treated hydrogel demonstrated 238 ± 14 bacteria colonies. The decreased bacteria colonies in PVA/TA@s-NC 4 treated hydrogel further suggested its antibacterial potential.

3.7. Electrochemical behaviors of hydrogel

Conductivity is required in the development of wearable electronic devices. The hydrogel conductivity was measured using a four-probe instrument, and the results are shown in Fig. 7a. The details of the hydrogel dimensions and their resistances are shown in Table S1. Enhanced conductivity ($6.05 \times 10^{-4} \rightarrow 3.16 \times 10^{-3}$ S/cm) was observed in the composite hydrogels compared to the pure polymer hydrogel,

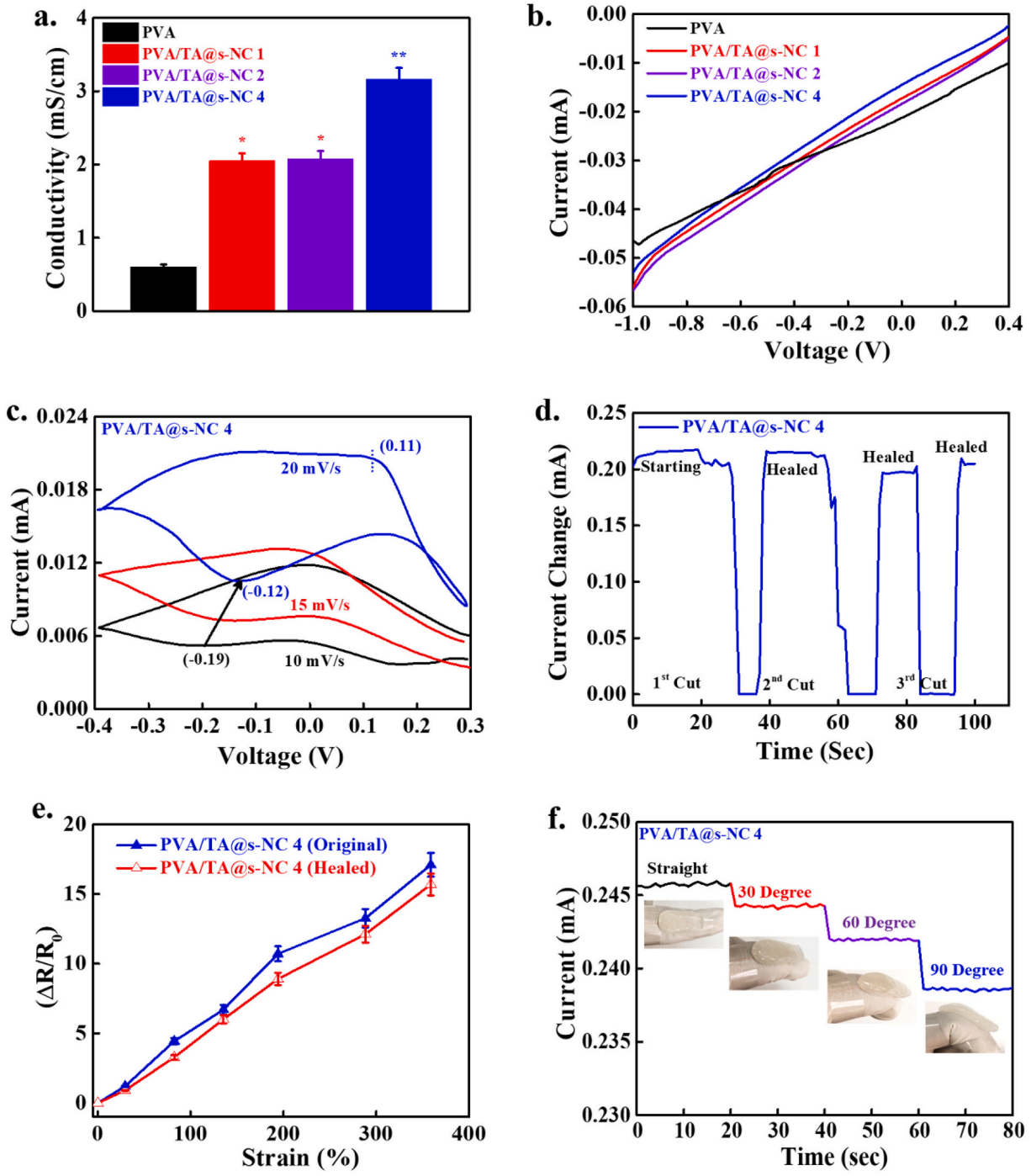

Fig. 7. Evaluation of the conductivity of the developed hydrogels at room temperature. (a) Conductivity value of the indicated hydrogels, (b) I-V curves of indicated hydrogels, (c) CV curves of the indicated hydrogel in measured regions, (d) change in current at different healing time, (e) change in the relative resistance of the indicated hydrogel with strain, and (f) change in the current of the hydrogel at different position of the human finger.

which increased with increasing TA@s-NC content in the polymer matrix, demonstrating the accelerating effects of TA@s-NC on the PVA conductivity. The high water content of the hydrogels assisted the ionization of TA@s-NC and the generation of free hydrogen ions. The generated ions migrate directionally at a specific voltage, enhancing the conductivity in the composite hydrogels. The PVA/TA@s-NC 4 hydrogel contains more ionized ions and conduction pathways than other hydrogels at a particular voltage, thereby improving conductivity. Enhanced electrical conductivity in a phytic acid-incorporated PVA hydrogel has been previously reported owing to the ionization of ions and the migration of hydrogen ions at a specific voltage [66]. The conductivity potential of the hydrogels was further examined by illuminating a light-emitting diode (LED) bulb. Here, we chose the PVA/TA@s-NC 4 hydrogel for the demonstration because of its enhanced conductivity compared to other hydrogels. The photographs of the LED bulbs connected to the hydrogel are shown in Fig. S11. No illumination was observed in the hydrogel-connected LED without an applied voltage, whereas bright illumination occurred under a specific voltage, indicating the conductive potential of the developed hydrogel. Current-voltage (I-V) measurements investigated the electrical conductance behavior of the developed hydrogels, and the results are shown in Fig. 7b. The I-V curves of the hydrogels were linear and non-hysteretic, indicating their electro-conductive properties. The conductance value was 0.0261, 0.0339, 0.0346, and 0.0351 mS for PVA, PVA/TA@s-NC 1, PVA/TA@s-NC 2, and PVA/TA@s-NC 4 hydrogels, respectively. The composite hydrogels exhibited better conductance behavior than the pure polymer, suggesting improved electro-conductive behavior. The improved electro-conductive behavior of the composite hydrogels was attributed to the formation of an effective ion transfer pathway in the hydrogels, which facilitated the transport of ions at the applied voltage [67]. The dimensions of the hydrogel used for the I-V measurements are given in Table S2.

The electrochemical behavior of the developed hydrogels was determined through cyclic voltammetry (CV) in an aqueous solution of sulfuric acid (1 mol/L) in the scan range of (−0.4)–(0.3) V, and the obtained CV curves are shown in Fig. 7c. Here, we chose the PVA/TA@s-NC 4 hydrogel to examine its electrochemical performance because of its superior conductivity compared to other hydrogels. The CV curves were nearly rectangular, with the redox peaks at −0.19 V and 0.11 V. The redox peaks in the hydrogel were attributed to the reduction in the abundance of hydroxyl groups in the hydrogel and the oxidation of the benzenoid structure of TA [68]. A noticeable increase in the peak currents was observed in the CV curves of the hydrogel with increasing scan rates, demonstrating good electrochemical responsiveness and rate capability. This behavior in the hydrogel may originate from enhanced ion transport in the measured regions. We also measured the change in the hydrogel current over three consecutive steps of the cutting and re-joining process to examine the effects of the self-healing process on the electrical properties of the hydrogel. The change in the current profile of the hydrogel is shown in Fig. 7d. A steady current was observed in the hydrogel, which rapidly decreased after cutting owing to the damage to the electrical pathway. However, the hydrogel regained its original current value after healing, indicating the regeneration of an effective electrical pathway through the self-healing process. The re-gaining of the initial current value in the healed hydrogel was due to the dynamic reversible interactions within the hydrogel components. Similar patterns were observed in three consecutive processes, demonstrating the appealing electrical properties of the hydrogel.

The self-healing efficiency of PVA/TA@s-NC 4 hydrogel was also investigated by monitoring the changes in the relative resistance of the original hydrogel and healed hydrogel. The results are presented in Fig. 7e. An enhancement in the resistance was observed with increased strain due to the weakening of the electrical conduction pathway. The healed hydrogel demonstrates similar behavior as the original, indicating the effective regeneration of the electrical pathway through the self-healing process. Additionally, we measured the change in the current of the hydrogel applied to the surface of the human finger under straight and different bending conditions (30°, 60°, and 90°), and the results are shown in Fig. 7f. No significant current change was observed in the hydrogel under static conditions because of the insignificant change in hydrogel resistance. However, a decrease in the current value occurred in the hydrogel with increasing the finger-bending magnitude. The decrease in the hydrogel current is attributed to the resistance enhancement during finger bending at a fixed voltage. An enhancement in the resistance of a conductive hydrogel by increasing the bending angles was previously reported [69].

3.8. Sensing efficiency and sensitivity of hydrogel

Based on the superior electrochemical performance of PVA/TA@s-NC 4 compared to other hydrogels, we analyzed the real-time strain-sensing ability of the hydrogel at different parts of the human body (finger, wrist, and knee motions). The stretching and bending processes were performed with human fingers to detect the real-time motion through the developed hydrogel, and the results are presented in Fig. 8a. The hydrogel strain sensor exhibits a steady deformation pattern during the stretching and bending of the finger, indicating its real-time motion-monitoring potential. The pattern of resistance change depends on the magnitude of the finger motion. A higher resistance change occurred during bending than stretching because of the decrease in the hydrogel current under bending, as observed in Fig. 7e. Furthermore, we measured the motion at the wrist and knee parts of the human body to explore the real-time strain-sensing efficiency of the developed hydrogel, and the corresponding resistance changes are shown in Fig. 8b–c. Nearly constant and rapid resistance changes were observed during the motion of the wrist and knee at a specific angle, suggesting its high sensitivity and good fidelity with the fast recovery of the sensor in monitoring the motion of the human body parts.

The real-time strain-sensing potential of the healed hydrogel was also examined on a human finger, and the obtained waveforms are shown in Fig. 8d. The healed hydrogel exhibits uniform waveforms during the motion of the human finger, which is identical to that of the original hydrogel, showing the motion-sensing potential of the healed hydrogel. The change in the generated waveforms was profoundly affected by the magnitude of the finger motion. Furthermore, we monitored the strain-sensing potential of the hydrogel under harsh conditions (−5 °C) to validate the anti-freezing potential of the hydrogel, and the obtained results are shown in Fig. 8e. The hydrogel exhibited a similar waveform under harsh conditions, indicating its strain-sensing potential under critical conditions. The generated waveforms were similar to those under normal finger motion conditions. The strain sensitivity of the hydrogels (original and healed) was examined in terms of gauge factor (GF) by measuring the electrical resistance change under applied strain conditions. The obtained data are presented in Fig. 8f. The GF value was 4.1 and 4.75 for the original hydrogel with 30 % and 360 % strain, respectively. The GF value was 3.05 and 4.3 for the healed hydrogel with 30 % and 360 % strain, respectively, showing a linear change in the relative resistance with strain. The developed hydrogel shows a better GF value than some previously reported PVA/nanocellulose-based hydrogels [70,71]. Moreover, the obtained GF values were lower than the hydrogels fabricated using conductive materials, such as carbon nanotubes and polyaniline [35,72,73].

However, the GF value can be further increased by integrating more conducting nanomaterials or polymer matrices. These results indicate that the developed hydrogel with multifunctional ability can be used as a strain sensor in real-time applications. A comparative study of some previously reported works based on PVA hydrogels with our work is given in Table 2 [42,74–79]. The developed hydrogels showed relatively improved physicochemical properties (toughness, viscoelasticity, and adhesiveness) than previously reported works for strain-sensing.

Furthermore, we showed the temperature-sensing potential of the developed hydrogels through a simple electric circuit at different

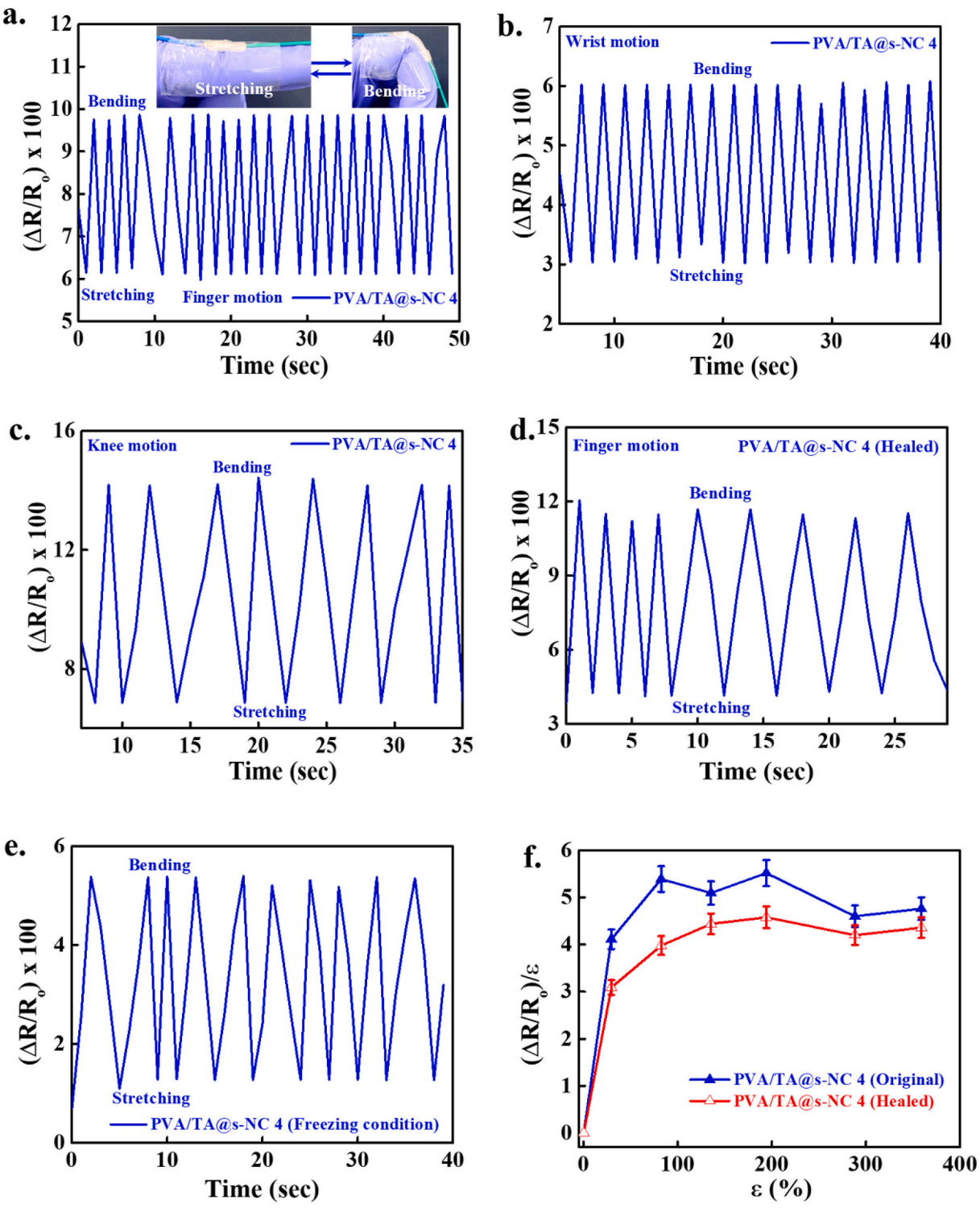

Fig. 8. Evaluation of the real-time sensing properties of the developed hydrogels at room temperature. (a) Change in resistance value of the indicated hydrogel during the stretching and bending of human finger, (b) change in the resistance of the indicated hydrogel during wrist motion, (c) change in the resistance value of the indicated hydrogel during knee motion of human leg, (d) change in resistance value of the healed hydrogel during the stretching and bending of human finger, (e) change in resistance value of the indicated hydrogel under harsh conditions, and (f) gauge factor of the original and healed hydrogels at different strain. All experiments were done in triplicate ($n = 3$).

temperatures (RT and −2 °C). It is believed that the conductivity of the developed hydrogels would decrease with decreasing the temperature due to the movement of the limited ions, leading to the enhancement in the circuit resistance [80]. The LED illumination behaviors at different temperatures are shown in Fig. S12. A bright illumination was observed at RT, whereas dimmed illumination occurred in ice due to increased circuit resistance. These findings show that the developed hydrogel can also be used as a temperature sensor.

4. Conclusion

The multifunctional hydrogels of polyvinyl alcohol/tannic acid-

Table 2
A comparative analysis of the previously reported PVA-based hydrogels with this work for strain sensing applications.

Components	Advantages	Limitations	Applications	Ref.
Polyvinyl alcohol/sodium alginate/tannic acid	Enhanced mechanical strength and conductivity	Adhesiveness not performed Low gauge factor (2.07)	Strain sensing	[74]
Polyvinyl alcohol/sodium alginate/tannic acid	Superior stretchability (780 %), rapid self-healing and high gauge factor (15.98)	Low adhesiveness	Strain sensing, and speech recognition ability	[75]
Polyvinyl alcohol/nanocellulose/carbon dots	Enhanced mechanical and self-healing potentials	Sensitivity value (gauge factor) not mentioned	Real time pressure and glucose sensing	[76]
Polyvinyl alcohol/polypyrrole functionalized nanocellulose	Superior mechanical and adhesive strength Good recovery potential	Low gauge factor (2.52)	Electronic skin sensors	[77]
Polyvinyl alcohol/nanocellulose/carbon nanotubes	Improved mechanical strength and conductivity Rapid self-healing and shape memory potential	Sensitivity value (gauge factor) not mentioned	Strain sensing	[78]
Polyvinyl alcohol/nanocellulose	Superior stretchability (1900 %), rapid healing (15 s), transparent, and conductive	Adhesiveness and gauge factor not evaluated	Strain and pressure sensing	[79]
Polyvinyl alcohol/tannic acid functionalized nanocellulose	Enhanced tensile strength, toughness (0.44 MJ/m^3), viscoelasticity, and conductivity	Moderate gauge factor (3.76)	Strain sensing, and speech recognition ability	[42]
Polyvinyl alcohol/tannic acid functionalized spherical nanocellulose	Superior stretchability (1211 %), toughness (13.39 MJ/m^3), and adhesiveness (59.6 kPa) Improved recovery, biocompatibility and conductivity with gauge factor 4.75	–	Strain and temperature sensing	This study

functionalized nanocellulose (PVA/TA@s-NC) were developed for strain-sensing applications. The hydrogels show improved viscoelasticity, recovery property, and adhesiveness. The developed hydrogels demonstrate ultra-stretchable and self-healing potentials, which are highly desirable for strain-sensing applications. Adding TA@s-NC to the polymer matrix improved the shape-memory behavior and conductivity of the developed hydrogels. The biocompatibility of the hydrogels was examined using HDF cells. No cytotoxicity was observed for the developed hydrogels, indicating biocompatibility. Furthermore, the hydrogels exhibited antibacterial potential against *E. coli*, providing additional advantages for developing sensing devices by suppressing bacterial growth.

The real-time sensing ability of the hydrogels was monitored on the surface of the human skin (finger, wrist, and knee motion). Steady deformation patterns were observed during the stretching and bending of the finger, wrist, and knee, indicating their real-time motion-monitoring potential. Further, the hydrogel exhibited strain-sensing potential under harsh conditions. The sensitivity of the developed hydrogel was monitored in terms of the gauge factor, and it was 4.75, showing good sensitivity. These findings indicate that the hydrogels have multifunctional characteristics and can be used to develop wearable electronic devices for sensing applications. The developed hydrogels also demonstrate temperature-sensing ability. However, more detailed studies are required to explore the other sensing abilities (humidity, pressure, *etc.*) of the developed hydrogels for desired applications.

CRedit authorship contribution statement

Dinesh K. Patel: Conceptualization, Methodology, Investigations, Data curation, Visualization, Formal analysis, Writing-original & Revised manuscript. Keya Ganguly, and Sayan Deb Dutta: Cytotoxicity evaluation. Tejal V. Patil: Antibacterial investigation. Aayushi Randhawa: Visualization and analysis. Ki-Taek Lim: Supervision, Funding acquisition, Project administration, Writing-review & editing.

Declaration of competing interest

The authors declare that they have no known competing financial interests or personal relationships that could have appeared to influence the work reported in this paper.

Data availability

The data used to support the findings of this study are available from the corresponding author upon request.

Acknowledgments

The Basic Science Research Program supported this work through the National Research Foundation of Korea (NRF) funded by the Ministry of Education (No. 2018R1A6A1A03025582, 2019R1D1A3A03103828, and 2022R1I1A3063302), Republic of Korea.

Appendix A. Supplementary data

Supplementary data to this article can be found online at https://doi.org/10.1016/j.ijbiomac.2022.12.286.

References

[1] R. Liu, H. Wang, W. Lu, L. Cui, S. Wang, Y. Wang, Q. Chen, Y. Guan, Y. Zhang, Highly tough, stretchable and resilient hydrogels strengthened with molecular springs and their application as a wearable, flexible sensor, Chem. Eng. J. 415 (2021), 128839.
[2] J. Ren, Y. Liu, Z. Wang, S. Chen, Y. Ma, H. Wei, S. Lü, An anti-swellable hydrogel strain sensor for underwater motion detection, Adv. Funct. Mater. 32 (2021), 2107404.
[3] S. Zeng, J. Zhang, G. Zu, J. Huang, Transparent, flexible, and multifunctional starch-based double-network hydrogels as high-performance wearable electronics, Carbohydr. Polym. 267 (2021), 118198.
[4] R. Jin, J. Xu, L. Duan, G. Gao, Chitosan-driven skin-attachable hydrogel sensors toward human motion and physiological signal monitoring, Carbohydr. Polym. 268 (2021), 118240.
[5] Y. Zhou, C. Wan, Y. Yang, H. Yang, S. Wang, Z. Dai, K. Ji, H. Jiang, X. Chen, Y. Long, Highly stretchable, elastic, and ionic conductive hydrogel for artificial soft electronics, Adv. Funct. Mater. 29 (2019), 1806220.
[6] D. Chen, X. Zhao, X. Wei, J. Zhang, D. Wang, H. Lu, P. Jia, Ultrastretchable, tough, antifreezing, and conductive cellulose hydrogel for wearable strain sensor, ACS Appl. Mater. Interfaces 12 (2020) 53247–53256.
[7] Q. Zhang, X. Liu, L. Duan, G. Gao, Ultra-stretchable wearable strain sensors based on skin-inspired adhesive, tough and conductive hydrogels, Chem. Eng. J. 365 (2019) 10–19.
[8] Y. Yang, N. Sun, Z. Wen, P. Cheng, H. Zheng, H. Shao, Y. Xia, C. Chen, H. Lan, X. Xie, C. Zhou, J. Zhong, X. Sun, S.-T. Lee, Liquid-metal-based super-stretchable and structure-designable triboelectric nanogenerator for wearable electronics, ACS Nano 12 (2018) 2027–2034.
[9] C.-H. Li, C. Wang, C. Keplinger, J.-L. Zuo, L. Jin, Y. Sun, P. Zheng, Y. Cao, F. Lissel, C. Linder, X.-Z. You, Z. Bao, A highly stretchable autonomous self-healing elastomer, Nat. Chem. 8 (2016) 618–624.
[10] Z. Zou, C. Zhu, Y. Li, X. Lei, W. Zhang, J. Xiao, Rehealable, fully recyclable, and malleable electronic skin enabled by dynamic covalent thermoset nanocomposite, Sci. Adv. 4 (2018) 508–516.
[11] K. Parida, G. Thangavel, G. Cai, X. Zhou, S. Park, J. Xiong, P.S. Lee, Extremely stretchable and self-healing conductor based on thermoplastic elastomer for all-three-dimensional printed triboelectric nanogenerator, Nat. Commun. 10 (2019) 2158–2167.
[12] Y. Chen, A.M. Kushner, G.A. Williams, Z. Guan, Multiphase design of autonomic self-healing thermoplastic elastomers, Nat. Chem. 4 (2012) 467–472.
[13] X. Yan, Z. Liu, Q. Zhang, J. Lopez, H. Wang, H.-C. Wu, S. Niu, H. Yan, S. Wang, T. Lei, J. Li, D. Qi, P. Huang, J. Huang, Y. Zhang, Y. Wang, G. Li, J.B.H. Tok, X. Chen, Z. Bao, Quadruple H-bonding cross-linked supramolecular polymeric

materials as substrates for stretchable, antitearing, and self-healable thin film electrodes, J. Am. Chem. Soc. 140 (2018) 5280–5289.
[14] H. Guo, Y. Han, W. Zhao, J. Yang, L. Zhang, Universally autonomous self-healing elastomer with high stretchability, Nat. Commun. 11 (2020) 2037–2046.
[15] N. Yang, P. Qi, J. Ren, H. Yu, S. Liu, J. Li, W. Chen, D.L. Kaplan, S. Ling, Polyvinyl alcohol/silk fibroin/borax hydrogel ionotronics: a highly stretchable, self-healable, and biocompatible sensing platform, ACS Appl. Mater. Interfaces 11 (2019) 23632–23638.
[16] A. Kumar, S.S. Han, PVA-based hydrogels for tissue engineering: a review, Int. J. Polym. Mater. Polym. Biomater. 66 (2016) 159–182.
[17] I. Erel-Unal, S.A. Sukhishvili, Hydrogen-bonded multilayers of a neutral polymer and a polyphenol, Macromolecules 41 (2008) 3962–3970.
[18] H. Fan, L. Wang, X. Feng, Y. Bu, D. Wu, Z. Jin, Supramolecular hydrogel formation based on tannic acid, Macromolecules 50 (2017) 666–676.
[19] D.K. Patel, S.D. Dutta, K.-T. Lim, Nanocellulose-based polymer hybrids and their emerging applications in biomedical engineering and water purification, RSC Adv. 9 (2019) 19143–19162.
[20] H. Luo, R. Cha, J. Li, W. Hao, Y. Zhang, F. Zhou, Advances in tissue engineering of nanocellulose-based scaffolds: a review, Carbohydr. Polym. 224 (2019), 115144.
[21] J. Han, H. Wang, Y. Yue, C. Mei, J. Chen, C. Huang, Q. Wu, X. Xu, A self-healable and highly flexible supercapacitor integrated by dynamically cross-linked electro-conductive hydrogels based on nanocellulose-templated carbon nanotubes embedded in a viscoelastic polymer network, Carbon 149 (2019) 1–18.
[22] Q. Ding, X. Xu, Y. Yue, C. Mei, C. Huang, S. Jiang, Q. Wu, J. Han, Nanocellulose-mediated electroconductive self-healing hydrogels with high strength, plasticity, viscoelasticity, stretchability, and biocompatibility toward multifunctional applications, ACS Appl. Mater. Interfaces 10 (2018) 27987–28002.
[23] X. Yang, S.K. Biswas, J. Han, S. Tanpichai, M.C. Li, C. Chen, S. Zhu, A.K. Das, H. Yano, Surface and interface engineering for nanocellulosic advanced materials, Adv. Mater. 33 (2020), 2002264.
[24] J. Han, Q. Ding, C. Mei, Q. Wu, Y. Yue, X. Xu, An intrinsically self-healing and biocompatible electroconductive hydrogel based on nanostructured nanocellulose-polyaniline complexes embedded in a viscoelastic polymer network towards flexible conductors and electrodes, Electrochim. Acta 318 (2019) 660–672.
[25] Z. Niu, W. Cheng, M. Cao, D. Wang, Q. Wang, J. Han, Y. Long, G. Han, Recent advances in cellulose-based flexible triboelectric nanogenerators, Nano Energy 87 (2021), 106175.
[26] L.S.F. Leite, C. Pham, S. Bilatto, H.M.C. Azeredo, E.D. Cranston, F.K. Moreira, L.H. C. Mattoso, J. Bras, Effect of tannic acid and cellulose nanocrystals on antioxidant and antimicrobial properties of gelatin films, ACS Sustain. Chem. Eng. 9 (2021) 8539–8549.
[27] J. Ru, Z. Wang, C. Tong, H. Liu, G. Wang, Z. Peng, Nonleachable antibacterial nanocellulose with excellent cytocompatible and UV-shielding properties achieved by counterion exchange with nature-based phenolic acids, ACS Sustain. Chem. Eng. 9 (2021) 15755–15767.
[28] D.K. Patel, K. Ganguly, J. Hexiu, S.D. Dutta, T.V. Patil, K.-T. Lim, Functionalized chitosan/spherical nanocellulose-based hydrogel with superior antibacterial efficiency for wound healing, Carbohydr. Polym. 284 (2022), 119202.
[29] Z. Hu, R.M. Berry, R. Pelton, E.D. Cranston, One-pot water-based hydrophobic surface modification of cellulose nanocrystals using plant polyphenols, ACS Sustain. Chem. Eng. 5 (2017) 5018–5026.
[30] S. Cometta, N. Bock, S. Suresh, T.R. Dargaville, D.W. Hutmacher, Antibacterial albumin-tannic acid coatings for scaffold-guided breast reconstruction, Front. Bioeng. Biotechnol. 9 (2021), 638577.
[31] M. Shabanian, M. Khaleghi, F. Allahyari, F. Attar, H.R. Ahmadi, M. Roohani, F. Seidi, H.A. Khonakdar, U. Wagenknecht, Tannic acid-modified tin oxide nanoparticle and aromatic polyamide: from synthesis to their application for preparation of safe p-PVC, Polym. Bull. 78 (2020) 1331–1352.
[32] Z. Hanif, Z.A. Khan, M.Z. Tariq, D. Choi, S.J. Park, Coatable tannic acid-deposited cellulose nanocrystals for Fe(III) sensing and its application to a facile, scalable and portable sensing platform, Dyes Pigments 196 (2021), 109732.
[33] H.M. Zidan, E.M. Abdelrazek, A.M. Abdelghany, A.E. Tarabiah, Characterization and some physical studies of PVA/PVP filled with MWCNTs, J. Mater. Res. Technol. 8 (2019) 904–913.
[34] D. Vanitha, S.A. Bahadur, N. Nallamuthu, A. Shunmuganarayanan, A. Manikandan, Studies on conducting polymer blends: synthesis and characterizations of PVA/PVP doped with CaCl2, J. Nanosci. Nanotechnol. 18 (2018) 1723–1729.
[35] S. Zhu, H. Sun, Y. Lu, S. Wang, Y. Yue, X. Xu, C. Mei, H. Xiao, Q. Fu, J. Han, Inherently conductive poly(dimethylsiloxane) elastomers synergistically mediated by nanocellulose/carbon nanotube nanohybrids toward highly sensitive, stretchable, and durable strain sensors, ACS Appl. Mater. Interfaces 13 (2021) 59142–59153.
[36] C. Zheng, K. Lu, Y. Lu, S. Zhu, Y. Yue, X. Xu, C. Mei, H. Xiao, Q. Wu, J. Han, A stretchable, self-healing conductive hydrogels based on nanocellulose supported graphene towards wearable monitoring of human motion, Carbohydr. Polym. 250 (2020), 116905.
[37] D.K. Patel, D. Rana, V.K. Aswal, S. Srivastava, P. Roy, P. Maiti, Influence of graphene on self-assembly of polyurethane and evaluation of its biomedical properties, Polymer 65 (2015) 183–192.
[38] M. Li, D. Chen, X. Sun, Z. Xu, Y. Yang, Y. Song, F. Jiang, An environmentally tolerant, highly stable, cellulose nanofiber-reinforced, conductive hydrogel multifunctional sensor, Carbohydr. Polym. 284 (2022), 119199.
[39] Y. Ye, Y. Zhang, Y. Chen, X. Han, F. Jiang, Cellulose nanofibrils enhanced, strong, stretchable, freezing-tolerant ionic conductive organohydrogel for multi-functional sensors, Adv. Funct. Mater. 30 (2020), 2003430.
[40] H.C. Oyeoka, C.M. Ewulonu, I.C. Nwuzor, C.M. Obele, J.T. Nwabanne, Packaging and degradability properties of polyvinyl alcohol/gelatin nanocomposite films filled water hyacinth cellulose nanocrystals, J. Bioresour. Bioprod. 6 (2021) 168–185.
[41] M. Chen, J. Chen, W. Zhou, J. Xu, C.-P. Wong, High-performance flexible and self-healable quasi-solid-state zinc-ion hybrid supercapacitor based on borax-crosslinked polyvinyl alcohol/nanocellulose hydrogel electrolyte, J. Mater. Chem. A 7 (2019) 26524–26532.
[42] H. Li, Y. Yang, M. Li, Y. Zhu, C. Zhang, R. Zhang, Y. Song, Frost-resistant and ultrasensitive strain sensor based on a tannic acid-nanocellulose/sulfonated carbon nanotube-reinforced polyvinyl alcohol hydrogel, Int. J. Biol. Macromol. 219 (2022) 199–212.
[43] W. Xing, Y. Tang, On mechanical properties of nanocomposite hydrogels: searching for superior properties, Nano Mater. Sci. 4 (2021) 83–96.
[44] J. Lee, B. Llerena Zambrano, J. Woo, K. Yoon, T. Lee, Recent advances in 1D stretchable electrodes and devices for textile and wearable electronics: materials, fabrications, and applications, Adv. Mater. 32 (2019), 1902532.
[45] L. Zhang, Z. Wang, C. Xu, Y. Li, J. Gao, W. Wang, Y. Liu, High strength graphene oxide/polyvinyl alcohol composite hydrogels, J. Mater. Chem. 21 (2011) 10399.
[46] S. Cho, S.Y. Hwang, D.X. Oh, J. Park, Recent progress in self-healing polymers and hydrogels based on reversible dynamic B-O bonds: boronic/boronate esters, borax, and benzoxaborole, J. Mater. Chem. A 9 (2021) 14630–14655.
[47] H. Bian, L. Wei, C. Lin, Q. Ma, H. Dai, J.Y. Zhu, Lignin-containing cellulose nanofibril-reinforced polyvinyl alcohol hydrogels, ACS Sustain. Chem. Eng. 6 (2018) 4821–4828.
[48] F. Pati, J. Jang, D.-H. Ha, S. Won Kim, J.-W. Rhie, J.-H. Shim, D.-H. Kim, D.-W. Cho, Printing three-dimensional tissue analogues with decellularized extracellular matrix bioink, Nat. Commun. 5 (2014) 3935.
[49] D.K. Patel, S.D. Dutta, W.-C. Shin, K. Ganguly, K.-T. Lim, Fabrication and characterization of 3D printable nanocellulose-based hydrogels for tissue engineering, RSC Adv. 11 (2021) 7466–7478.
[50] D.K. Patel, K. Ganguly, S.D. Dutta, T.V. Patil, K.-T. Lim, Multifunctional hydrogels of polyvinyl alcohol/polydopamine functionalized with carbon nanomaterials as flexible sensors, Mater. Today Commun. 32 (2022), 103906.
[51] Y. Qin, J. Wang, C. Qiu, X. Xu, Z. Jin, A dual cross-linked strategy to construct moldable hydrogels with high stretchability, good self-recovery, and self-healing capability, J. Agri. Food Chem. 67 (2019) 3966–3980.
[52] S. Das, P. Martin, G. Vasilyev, R. Nandi, N. Amdursky, E. Zussman, Processable, ion-conducting hydrogel for flexible electronic devices with self-healing capability, Macromolecules 53 (2020) 11130–11141.
[53] Z. Deng, T. Hu, Q. Lei, J. He, P.X. Ma, B. Guo, Stimuli-responsive conductive nanocomposite hydrogels with high stretchability, self-healing, adhesiveness, and 3D printability for human motion sensing, ACS Appl. Mater. Interfaces 11 (2019) 6796–6808.
[54] J. Chen, Q. Peng, T. Thundat, H. Zeng, Stretchable, injectable, and self-healing conductive hydrogel enabled by multiple hydrogen bonding toward wearable electronics, Chem. Mater. 31 (2019) 4553–4563.
[55] Y. Jiao, Y. Lu, K. Lu, Y. Yue, X. Xu, H. Xiao, J. Li, J. Han, Highly stretchable and self-healing cellulose nanofiber-mediated conductive hydrogel towards strain sensing application, J. Colloid Interface Sci. 597 (2021) 171–181.
[56] A. Phadke, C. Zhang, B. Arman, C.-C. Hsu, R.A. Mashelkar, A.K. Lele, M.J. Tauber, G. Arya, S. Varghese, Rapid self-healing hydrogels, Proc. Natl. Acad. Sci. 109 (2012) 4383–4388.
[57] Y. Zhang, Q. Chen, Z. Dai, Y. Dai, F. Xia, X. Zhang, Nanocomposite adhesive hydrogels: from design to application, J. Mater. Chem. B 9 (2021) 585–593.
[58] L. Zhao, J. Zhao, F. Zhang, Z. Xu, F. Chen, Y. Shi, C. Hou, Y. Huang, C. Lin, R. Yu, W. Guo, Highly stretchable, adhesive, and self-healing silk fibroin-dopted hydrogels for wearable sensors, Adv. Healthc. Mater. 10 (2021), 2002083.
[59] J. Shang, X. Le, J. Zhang, T. Chen, P. Theato, Trends in polymeric shape memory hydrogels and hydrogel actuators, Polym. Chem. 10 (2019) 1036–1055.
[60] X. Xiong, J. Sun, D. Hu, C. Xiao, J. Wang, Q. Zhuo, C. Qin, L. Dai, Fabrication of polyvinyl alcohol hydrogels with excellent shape memory and ultraviolet-shielding behavior via the introduction of tea polyphenols, RSC Adv. 10 (2020) 35226–35234.
[61] Y.-N. Chen, L. Peng, T. Liu, Y. Wang, S. Shi, H. Wang, Poly(vinyl alcohol)–tannic acid hydrogels with excellent mechanical properties and shape memory behaviors, ACS Appl. Mater. Interfaces 8 (2016) 27199–27206.
[62] H. Gao, Z. Zhao, Y. Cai, J. Zhou, W. Hua, L. Chen, L. Wang, J. Zhang, D. Han, M. Liu, L. Jiang, Adaptive and freeze-tolerant heteronetwork organohydrogels with enhanced mechanical stability over a wide temperature range, Nat. Commun. 8 (2017) 15911.
[63] Y. Wang, S. Liu, Q. Wang, X. Ji, X. An, H. Liu, Y. Ni, Nanolignin filled conductive hydrogel with improved mechanical, anti-freezing, UV-shielding and transparent properties for strain sensing application, Int. J. Biol. Macromol. 205 (2022) 442–451.
[64] N. Sahiner, S. Sagbas, M. Sahiner, C. Silan, N. Aktas, M. Turk, Biocompatible and biodegradable poly(tannic acid) hydrogel with antimicrobial and antioxidant properties, Int. J. Biol. Macromol. 82 (2016) 150–159.
[65] S. Li, S. Dong, W. Xu, S. Tu, L. Yan, C. Zhao, J. Ding, X. Chen, Antibacterial hydrogels, Adv. Sci. 5 (2018), 1700527.
[66] S. Zhang, Y. Zhang, B. Li, P. Zhang, L. Kan, G. Wang, H. Wei, X. Zhang, N. Ma, One-step preparation of a highly stretchable, conductive, and transparent poly(vinyl alcohol)–phytic acid hydrogel for casual writing circuits, ACS Appl. Mater. Interfaces 11 (2019) 32441–32448.
[67] H. Wang, S.K. Biswas, S. Zhu, Y. Lu, Y. Yue, J. Han, X. Xu, Q. Wu, H. Xiao, Self-healable electro-conductive hydrogels based on core-shell structured

nanocellulose/carbon nanotubes hybrids for use as flexible supercapacitors, Nanomaterials 10 (2020) 112.
[68] M.M. Abudabbus, I. Jevremović, K. Nešović, A. Perić-Grujić, K.Y. Rhee, V. Mišković-Stanković, In situ electrochemical synthesis of silver-doped poly(vinyl alcohol)/graphene composite hydrogels and their physico-chemical and thermal properties, Compos. B: Eng. 140 (2018) 99–107.
[69] X. Liu, Y. Ma, X. Zhang, J. Huang, Cellulose nanocrystal reinforced conductive nanocomposite hydrogel with fast self-healing and self-adhesive properties for human motion sensing, Colloids Surf. A: Physicochem. Eng. Asp. 613 (2021), 126076.
[70] L. Zhang, C. Wan, J. Su, C. Zhang, S. Wei, W. Tian, X. Liu, W. Cheng, X. Li, X. Li, X. Guo, K.-T. Yong, Y. Wu, A dual-crosslinked self-healing and antibacterial nanocellulose hydrogel for monitoring of human motions, Mater. Des. 215 (2022), 110464.
[71] J. Hu, Y. Wu, Q. Yang, Q. Zhou, L. Hui, Z. Liu, F. Xu, D. Ding, One-pot freezing-thawing preparation of cellulose nanofibrils reinforced polyvinyl alcohol based ionic hydrogel strain sensor for human motion monitoring, Carbohydr. Polym. 275 (2022), 118697.
[72] Y. Lu, Y. Yue, Q. Ding, C. Mei, X. Xu, Q. Wu, H. Xiao, J. Han, Self-recovery, fatigue-resistant, and multifunctional sensor assembled by a nanocellulose/carbon nanotube nanocomplex-mediated hydrogel, ACS Appl. Mater. Interfaces 13 (2021) 50281–50297.
[73] J. Han, K. Lu, Y. Yue, C. Mei, C. Huang, Q. Wu, X. Xu, Nanocellulose-templated assembly of polyaniline in natural rubber-based hybrid elastomers toward flexible electronic conductors, Ind. Crop. Prod. 128 (2019) 94–107.
[74] Y. Zhan, Y. Xing, Q. Ji, X. Ma, Y. Xia, Strain-sensitive alginate/polyvinyl alcohol composite hydrogels with janus hierarchy and conductivity mediated by tannic acid, Int. J. Biol. Macromol. 212 (2022) 202–210.
[75] L. Zhao, Z. Ren, X. Liu, Q. Ling, Z. Li, H. Gu, A multifunctional, self-healing, self-adhesive, and conductive sodium alginate/poly(vinyl alcohol) composite hydrogel as a flexible strain sensor, ACS Appl. Mater. Interfaces 13 (2021) 11344–11355.
[76] Z. Wang, F. Cheng, H. Cai, X. Li, J. Sun, Y. Wu, N. Wang, Y. Zhu, Robust versatile nanocellulose/polyvinyl alcohol/carbon dot hydrogels for biomechanical sensing, Carbohydr. Polym. 259 (2021), 117753.
[77] L. Han, S. Cui, H.-Y. Yu, M. Song, H. Zhang, N. Grishkewich, C. Huang, D. Kim, K. M.C. Tam, Self-healable conductive nanocellulose nanocomposites for biocompatible electronic skin sensor systems, ACS Appl. Mater. Interfaces 11 (2019) 44642–44651.
[78] G. Xiao, Y. Wang, H. Zhang, Z. Zhu, S. Fu, Cellulose nanocrystal mediated fast self-healing and shape memory conductive hydrogel for wearable strain sensors, Int. J. Biol. Macromol. 170 (2021) 272–283.
[79] X. Jing, H. Li, H.-Y. Mi, Y.-J. Liu, P.-Y. Feng, Y.-M. Tan, L.-S. Turng, Highly transparent, stretchable, and rapid self-healing polyvinyl alcohol/cellulose nanofibril hydrogel sensors for sensitive pressure sensing and human motion detection, Sensors Actuators B Chem. 295 (2019) 159–167.
[80] J. Min, Z. Zhou, J. Zheng, C. Yan, H. Sha, M. Hong, H. Fu, Self-healing, water-retaining, antifreeze, conductive PVA/PAA-PAM-IS/GC composite hydrogels for strain and temperature sensors, Macromol. Mater. Eng. 307 (2022), 2100948.